ARTICLES
https://doi.org/10.1038/s41556-021-00672-3
nature cell biology



# LIMIT is an immunogenic lncRNA in cancer immunity and immunotherapy

Gaopeng Li[1,2], Ilona Kryczek[1,2], Jutaek Nam[3], Xiong Li[1,2], Shasha Li[1,2], Jing Li[1,2], Shuang Wei[1,2], Sara Grove[1,2], Linda Vatan[1,2], Jiajia Zhou[1,2], Wan Du[1,2], Heng Lin[1,2], Ton Wang[1], Chitra Subramanian[1], James J. Moon[3,4], Marcin Cieslik[5,6], Mark Cohen[1,4,7] and Weiping Zou[1,2,6,8,9] ✉

**Major histocompatibility complex-I (MHC-I) presents tumour antigens to CD8$^+$ T cells and triggers anti-tumour immunity. Humans may have 30,000–60,000 long noncoding RNAs (lncRNAs). However, it remains poorly understood whether lncRNAs affect tumour immunity. Here, we identify a lncRNA, lncRNA inducing MHC-I and immunogenicity of tumour (LIMIT), in humans and mice. We found that IFNγ stimulated LIMIT, LIMIT *cis*-activated the guanylate-binding protein (GBP) gene cluster and GBPs disrupted the association between HSP90 and heat shock factor-1 (HSF1), thereby resulting in HSF1 activation and transcription of MHC-I machinery, but not PD-L1. RNA-guided CRISPR activation of *LIMIT* boosted GBPs and MHC-I, and potentiated tumour immunogenicity and checkpoint therapy. Silencing *LIMIT*, GBPs and/or HSF1 diminished MHC-I, impaired antitumour immunity and blunted immunotherapy efficacy. Clinically, LIMIT, GBP- and HSF1-signalling transcripts and proteins correlated with MHC-I, tumour-infiltrating T cells and checkpoint blockade response in patients with cancer. Together, we demonstrate that LIMIT is a cancer immunogenic lncRNA and the LIMIT–GBP–HSF1 axis may be targetable for cancer immunotherapy.**

Checkpoint blockade unleashes CD8$^+$ T cell-mediated immune power against cancer[1]. MHC-I has a key role in CD8$^+$ T-cell priming and activation[2]. However, MHC-I is frequently downregulated in cancer cells, resulting in tumour immune evasion and immunotherapy resistance[3,4]. It is important to understand how to recover tumour MHC-I expression and revitalize the antitumour immune response[5].

lncRNAs are emerging rapidly along with the advance in deep RNA sequencing, covering many more loci in the human genome than protein-coding genes[6]. lncRNAs regulate protein-coding genes at multiple levels[7–9] and have pivotal roles in genomic imprinting[10], cell differentiation[11] and cancer progression[12]. However, the identity, mode of action, function and clinical relevance of specific lncRNAs in cancer immunity and immunotherapy remain unknown.

In this Article, we identify LIMIT as a cancer immunogenic lncRNA. LIMIT affects MHC-I machinery and antitumour immunity. We found that LIMIT locally targets GBPs, thereby forming a molecular cascade of LIMIT–GBP–HSF1–MHC to alter antitumour immunity and the efficacy of tumour immunotherapy. Our research not only reveals the biology of the immunogenic lncRNA LIMIT, but also suggests that the LIMIT–GBP–HSF1 axis may be targetable for cancer immunotherapy.

## LIMIT is an immunogenic lncRNA

To examine unknown regulatory genes in tumour immunity, on the basis of tumour CD8$^+$ T-cell infiltration, we divided human melanoma (TCGA, SKCM) into hot and cold tumour types and analysed immunogenic gene correlations. In addition to *CD8A*, *IFNG* and MHC-I-related (*HLA-ABC*) transcripts, we found that a lncRNA candidate was enriched in hot tumours, among 3,926 lncRNA candidates annotated by GENCODE[13] (Fig. 1a and Supplementary Table 1). On the basis of functional studies in the following experiments, we designated this lncRNA candidate as lncRNA inducing MHC-I and immunogenicity of tumour (LIMIT). In a human melanoma dataset, the levels of *LIMIT* were positively correlated with the levels of *IFNG*, MHC-I and *CD8A* (Fig. 1b–d). Consistent with this, gene-set enrichment analysis (GSEA) revealed that *LIMIT* expression was correlated with IFNγ response genes, antigen presentation through MHC-I and immune activation (Fig. 1e–h). Moreover, the levels of *LIMIT* were correlated with enhanced checkpoint immunotherapy response rates[14–17] (Fig. 1i) and were associated with survival in patients with melanoma (Fig. 1j). Furthermore, the expression of *LIMIT* was correlated with *IFNG*, MHC-I and *CD8A* across multiple cancer types (Extended Data Fig. 1a–l). Thus, LIMIT is a potential immunogenic lncRNA.

We validated whether LIMIT is a lncRNA. Northern blotting showed that LIMIT was approximately 2 kb in length in human A375 melanoma cells (Fig. 1k). We applied rapid amplification of cDNA ends (RACE) and characterized the cDNA ends of *LIMIT* in both human (A375) and mouse (B16) melanoma cells (Fig. 1l,m). We next cloned full-length *LIMIT* of both humans and mice, and aligned with corresponding genome sequences (Extended Data Fig. 2a,b). Human *LIMIT* is located in chromosome 1, with 1,967 nucleotides and 6 exons (Extended Data Fig. 2a), whereas mouse *Limit* is located in chromosome 3, with 1,634 nucleotides and 7 exons (Extended Data Fig. 2b). *LIMIT* does not contain a valid Kozak sequence. When we prepared RNA from nuclear and cytoplasmic fractions of A375 cells, LIMIT was mainly detected in the

[1]Department of Surgery, University of Michigan, Ann Arbor, MI, USA. [2]Center of Excellence for Cancer Immunology and Immunotherapy, University of Michigan Rogel Cancer Center, Ann Arbor, MI, USA. [3]Department of Pharmaceutical Sciences, University of Michigan, Ann Arbor, MI, USA. [4]Department of Biomedical Engineering, University of Michigan, Ann Arbor, MI, USA. [5]Department of Computational Medicine & Bioinformatics, University of Michigan, Ann Arbor, MI, USA. [6]Department of Pathology, University of Michigan, Ann Arbor, MI, USA. [7]Department of Pharmacology, University of Michigan, Ann Arbor, MI, USA. [8]Graduate Programs in Immunology, University of Michigan, Ann Arbor, MI, USA. [9]Tumor Biology, University of Michigan, Ann Arbor, MI, USA. ✉e-mail: wzou@med.umich.edu

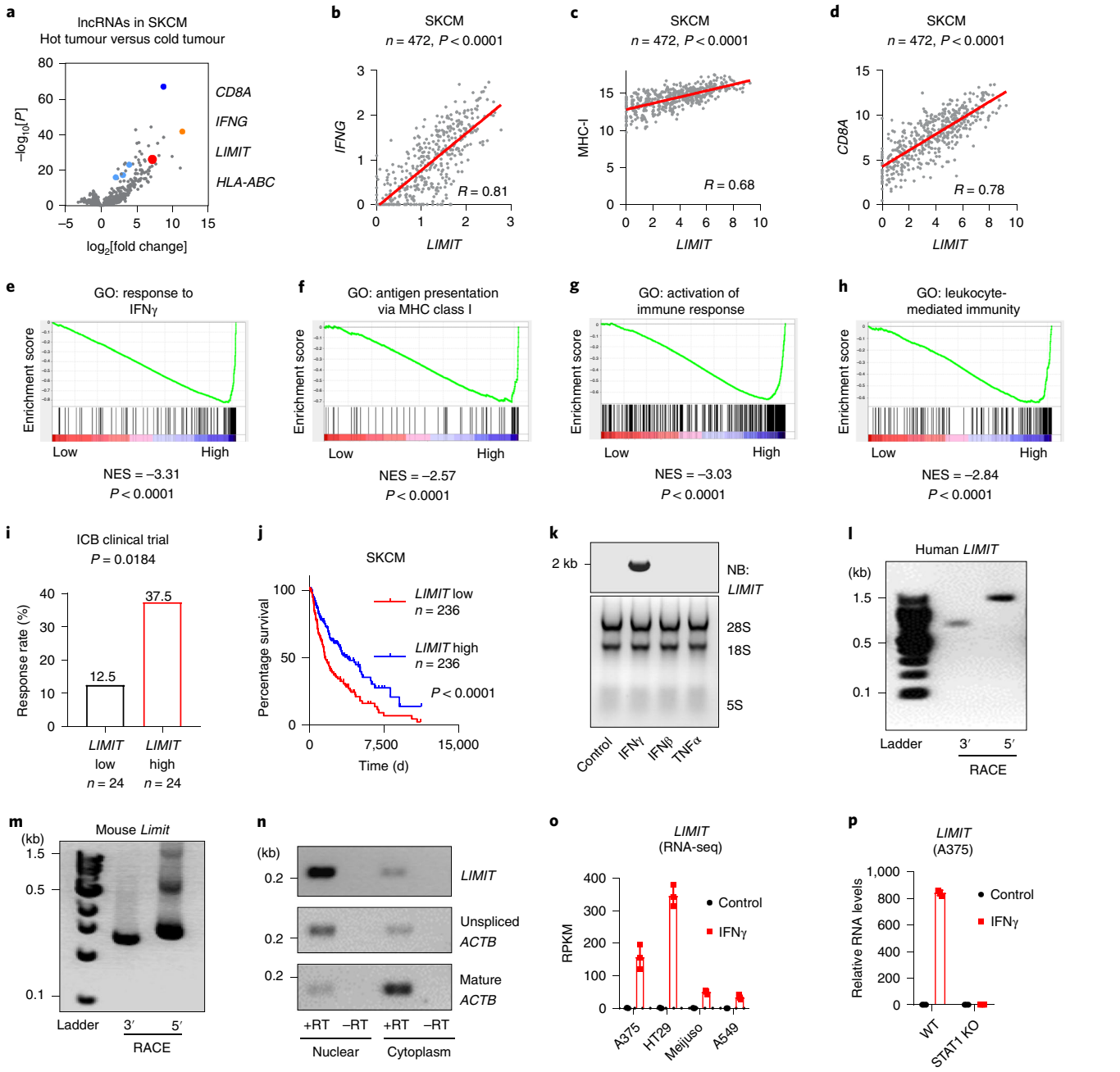


**Fig. 1 | LIMIT is an immunogenic lncRNA. a**, Human melanoma samples (TCGA dataset, SKCM, $n = 472$ patients) were divided into hot and cold tumours on the basis of *CD8A* transcripts. The volcano plots show the fold changes and *P* values of 3,926 lncRNA candidates in hot tumours (*CD8A*, top 10%) versus cold tumours (*CD8A*, bottom 10%). Statistical analysis was performed using two-sided *t*-tests. **b**–**d**, Correlation of *LIMIT* with *IFNG* (**b**), MHC-I (**c**) or *CD8A* (**d**) in patients with melanoma (TCGA, SKCM). Statistical analysis was performed using two-sided linear regression. **e**–**h**, Human melanoma samples (TCGA, SKCM) were divided into high ($n = 236$ patients) and low ($n = 236$ patients) *LIMIT* tumours. GSEA showed the indicated gene signatures. The following gene signatures were enriched in high LIMIT tumours: response to IFNγ (**e**), antigen presentation via MHC-I (**f**), activation of immune response (**g**), and leukocyte-mediated immunity (**h**). Statistical analysis was performed using GSEA analysis. GO, Gene Ontology. NES, normalized enrichment score. **i**, Patients with cancer who had received immune checkpoint blockade (ICB) therapy were divided into low and high *LIMIT* groups (the bottom 15% versus top 15%). The response rates to immune checkpoint blockade were calculated as the percentages of partial response (PR) plus complete response (CR). Statistical analysis was performed using $\chi^2$ tests. Patients were from four cohorts. **j**, Survival plot of patients with melanoma (TCGA, SKCM). Patients were divided into high ($n = 236$ patients) and low ($n = 236$ patients) LIMIT groups. Statistical analysis was performed using two-sided log-rank tests. **k**, A375 cells were treated with the indicated cytokines (5 ng ml$^{-1}$) for 24 h. LIMIT was detected using northern blotting (NB). The 28S rRNA, 18S rRNA and 5S rRNA are shown as loading controls. One out of two experiments is shown. **l**,**m**, 5′RACE and 3′RACE analysis of human LIMIT (**l**) or murine Limit (**m**). One out of two experiments is shown. **n**, A375 cells were treated with IFNγ for 24 h. LIMIT was detected using RT–PCR in nuclear or cytoplasmic RNAs. Unspliced *ACTB* and mature *ACTB* were used as controls for nuclear and cytoplasmic RNAs, respectively. One out of two experiments is shown. **o**, Reads per kb of transcript per million mapped reads (RPKM) of *LIMIT* in different cancer cells in response to IFNγ. **p**, WT or STAT1-KO A375 cells were treated with 5 ng ml$^{-1}$ IFNγ for 24 h. RNA levels of LIMIT were quantified using RT–qPCR. All data are mean ± s.d. For **o** and **p**, $n = 3$ biological independent samples. Source data are available online.

nuclear fraction (Fig. 1n). Thus, LIMIT has no protein-coding potential. Collectively, LIMIT meets all of the criteria to be defined as a lncRNA. Notably, at the *LIMIT* locus, a lncRNA candidate, pseudogene of *GBP1* (*GBP1P1*) was found in hepatocellular carcinoma[18]. However, *LIMIT* exhibited low similarities to *GBP1P1* or *GBP1* (Extended Data Fig. 2c and Supplementary Table 2). Thus, *LIMIT* is not *GBP1P1*.

A high correlation between *LIMIT* and IFNγ-responsive gene signature (Fig. 1e) suggests that IFNγ may stimulate *LIMIT* expression. Indeed, treatment with IFNγ induced the expression of *LIMIT*, as shown by northern blotting (Fig. 1k) and RNA-sequencing (RNA-seq) analysis in A375, HT29, Meijuso and A549 cells (Fig. 1o). However, treatment with other cytokines, such as IFNβ and TNFα, failed to induce *LIMIT* expression (Fig. 1k). Moreover, IFNγ failed to induce LIMIT in STAT1-knockout (KO) A375 cells (Fig. 1p). Thus, LIMIT is an IFNγ-responsive lncRNA in both human and mouse cells.

## LIMIT augments MHC-I expression

To study the function of LIMIT in tumour cells, we first knocked down *LIMIT* with small hairpin RNAs (shLIMIT). We used the BLAST tool to select *LIMIT* shRNAs that had no off-target candidates (Supplementary Tables 3–6). shLIMIT did not target GBP-coding genes (Extended Data Fig. 3a). In A375 cells, shLIMIT suppressed *LIMIT* expression (Fig. 2a), but had no effect on the phosphorylation of STAT1 (Fig. 2b) in response to IFNγ—suggesting that LIMIT did not affect the global IFNγ gene signalling. MHC-I and *CD274* (encoding PD-L1) are IFNγ-target genes[19–21]. ShLIMIT led to a decrease in the expression of MHC-I (Fig. 2c), but not PD-L1 (Extended Data Fig. 3b), in response to IFNγ stimulation. Consistent with this human data, silencing *Limit* in murine melanoma cell YUMM1.7 or colon cancer cell CT26 resulted in reduced MHC-I expression in response to IFNγ (Fig. 2d–g). In A375 cells, shLIMIT affected not only MHC-I expression (*HLA-ABC*, *HLA-E* and *HLA-F*), but also MHC-II expression (*HLA-DRA* and *HLA-DMA*), whereas LIMIT did not alter other IFNγ-signalling gene expression (Extended Data Fig. 3c). Thus, LIMIT participates in the regulation of IFNγ-induced MHC-I and MHC-II expression without altering the global IFNγ signalling pathway.

*LIMIT* is an interrupted gene with large introns, occupying around 17 kb in the genome. We failed to knock out the *LIMIT* locus using paired sgRNAs and Cas9. Given that there are five predicted STAT1/IRF1-binding sites in the *LIMIT* promoter, we designed four paired sgRNAs to delete these binding sites in the *LIMIT* promoter (Extended Data Fig. 3d). We generated A375 cells with the *LIMIT*-promoter deletion in all four combinations of sgRNAs. We found that IFNγ was no longer efficient at inducing the expression of *LIMIT* and MHC-I in tumour cells with the *LIMIT* promoter deletion compared with in wild-type (WT) cells (Fig. 2h,i).

We also used an RNA-guided CRISPR activation system to activate *Limit* expression in tumour cells[22]. We established four guide RNAs targeting the promoter region of *Limit* (sgLimit), and co-expressed with dCas9–VPR, a tripartite transcriptional activator fused with nuclease-null Cas9, into B16 cells (Extended Data Fig. 4a). All four sgLimit guide RNAs enhanced the expression of *Limit*, as well as MHC-I (Extended Data Fig. 4b,c). When we transfected B16 cells with pooled sgLimit and non-targeting sgRNAs (sgNT), sgLimit induced the expression of *Limit* and MHC-I, but not PD-L1 (Fig. 2j,k). Thus, Limit selectively targets MHC-I, but not PD-L1. Together, the loss- and gain-of-function experiments demonstrate that LIMIT can alter MHC-I expression in multiple cancer cells across mice and humans by 1.5−3-fold.

We next investigated whether LIMIT-altered MHC-I expression impacts TAA-specific $CD8^+$ T-cell-mediated tumour killing in vitro. To this end, we first genetically knocked down *B2M* using specific shRNAs (shB2M) in ovalbumin (OVA)-expressing B16 cells. shB2M resulted in a 1.5-fold reduction in OVA–$H2K^b$ expression (Extended Data Fig. 4d). When B16-OVA cells carrying shFluc and shB2M were incubated with OT-I cells, we observed a decrease in OT-I-mediated shB2M-B16-OVA cell killing compared with shFluc-B16-OVA cells (Extended Data Fig. 4e–g). The data suggest that 1.5–3-fold changes in MHC-I expression controlled by LIMIT could be functionally relevant in affecting TAA-specific CTL activities. To validate this, we activated *Limit* in B16-OVA cells expressing shFluc and shB2M. As expected, CRISPR activation of *Limit* induced minimal MHC-I expression in shB2M cells compared with in control cells (Fig. 2l). Accordingly, OT-I cells mediated minimal tumour killing in shB2M-OVA-B16 cells compared with in control cells (Fig. 2m,n). The data suggest that LIMIT-induced MHC-I expression is important in TAA-specific T-cell activation and function.

Antigen presenting cells (APCs), including macrophages and dendritic cells (DCs), express MHC-I and present antigens to and activate TAA-specific T cells. We extended our studies from tumour cells to APCs. IFNγ potently stimulated *Limit* expression in bone-marrow-derived DCs and macrophages (Extended Data Fig. 4h,i). We transfected macrophages with 5′FAM-labelled short interfering RNA targeting *Limit* (siLimit). Knocking down *Limit* resulted in lower MHC-I expression in response to IFNγ stimulation compared with the control (Extended Data Fig. 4j,k). Thus, LIMIT is an IFNγ-responsive lncRNA that can promote MHC-I expression in both tumour cells and APCs.

## LIMIT enhances anti-tumour immunity

Insufficient MHC-I expression confers tumour immune evasion and immunotherapy resistance[3]. To understand a role of Limit in antitumour immune responses in vivo, we inoculated control (shFluc) and *Limit*-silencing (shLimit) YUMM1.7 tumour cells into NOD scid γc-deficient (NSG, immune deficient) and WT C57BL/6 (immune competent) mice. Compared with control tumours, shLimit YUMM1.7 tumours grew comparably in NSG mice (Fig. 3a), whereas the tumours progressed faster in WT mice (Fig. 3b). Furthermore, we inoculated shLimit CT26 tumours into WT BALB/c mice. Again, silencing *Limit* resulted in enhanced CT26 tumour growth in the immune competent model (Fig. 3c). The data suggest that silencing *Limit* may impair anti-tumour immunity and facilitate tumour growth in an immune-dependent manner. In support of this, we detected a reduction of $CD3^+$, $IFN\gamma^+$ and $TNF\alpha^+$ T cells in the shLimit YUMM1.7 tumours (Fig. 3d,e). Together, silencing *Limit* impairs anti-tumour immunity.

To determine the expression of MHC-I and MHC-I–SIINFEKL in vivo, we established YUMM1.7 cells stably expressing OVA (YUMM1.7-OVA), and transduced them with shRNA targeting *Limit* or Fluc. After IFNγ treatment, we detected reduced surface expression of OVA–$H2K^b$ in shLimit-YUMM1.7 cells (Extended Data Fig. 5a). We inoculated shLimit-YUMM1.7-OVA cells and shFluc-YUMM1.7-OVA cells into C57BL/6 mice. We next dissected tumour tissues and detected the expression of $H2D^b$ and OVA–$H2K^b$ in tumour cells. We observed a reduction of $H2D^b$ and OVA–$H2K^b$ in shLimit-YUMM1.7-OVA cells compared with in the control cells (Extended Data Fig. 5b–f). The data indicate that Limit may affect MHC-I and MHC-I–antigen expression in vivo.

We also inoculated control (sgNT) and *Limit*-activating (sgLimit) B16 cells into WT C57/BL6 mice. As expected, sgLimit (*Limit* activation) substantially reduced tumour growth (Fig. 3f). This was accompanied by an increase in tumour-infiltrating T-cell numbers and activation (Fig. 3g,h). B16 melanoma is a relatively insensitive tumour model to PD-L1 blockade[23]. Consistent with this, PD-L1 blockade failed to control sgNT B16 tumour growth in mice. Interestingly, *Limit* activation in B16 tumours with sgLimit sensitized the tumour response to PD-L1 blockade, as shown by a reduction in tumour progression (Fig. 3i). Together,

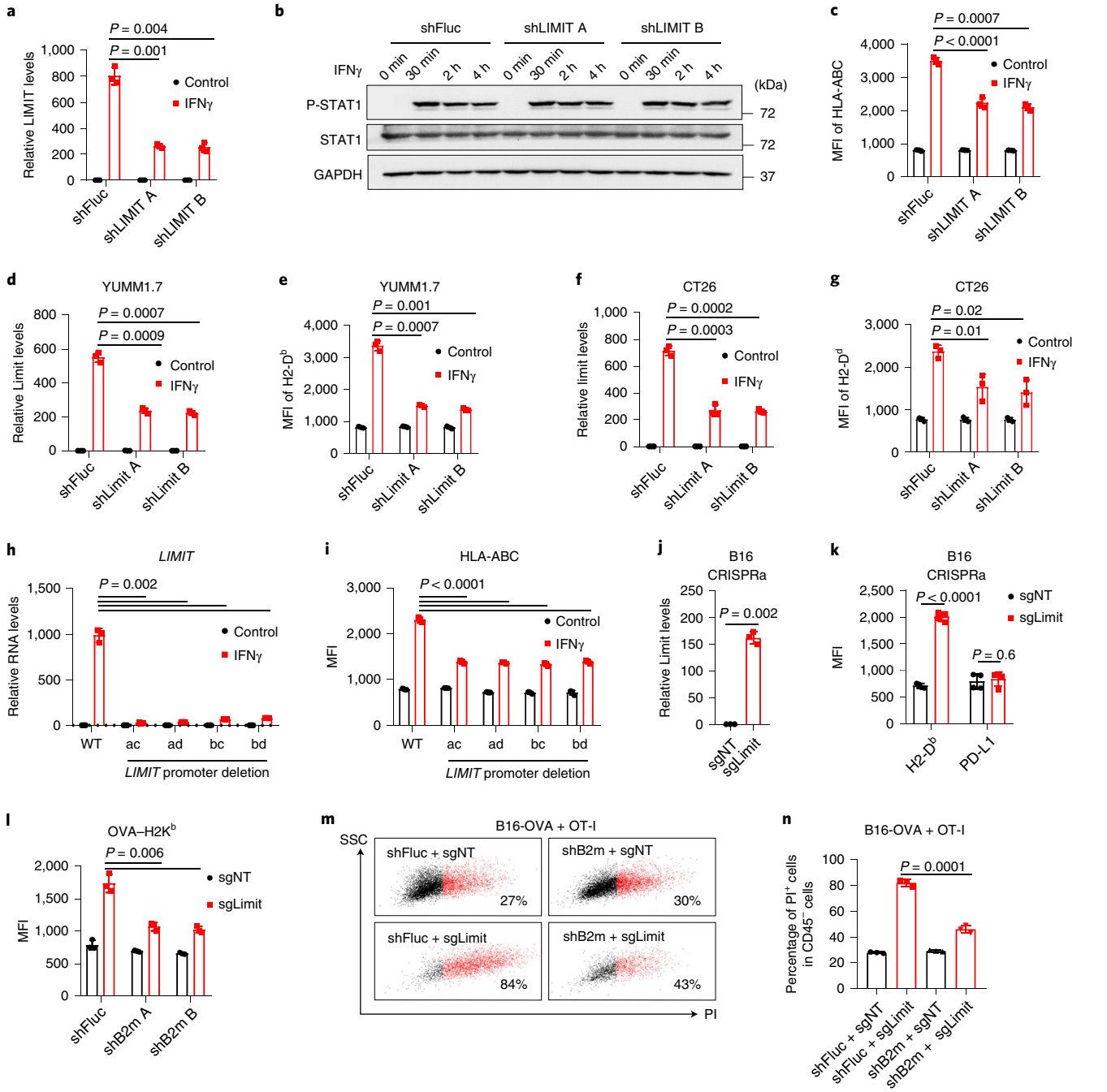


**Fig. 2 | LIMIT augments MHC-I expression. a**, A375 shFluc or shLIMIT cells were treated with IFNγ for 24 h. RNA levels of LIMIT were determined using RT–qPCR. Statistical analysis was performed using two-sided *t*-tests. **b**, A375 shFluc or shLIMIT cells were treated with IFNγ for the indicated time. Protein levels of phosphorylated STAT1 (p-Y701), STAT1 and GAPDH were determined using western blotting. One out of two experiments is shown. **c**, A375 shFluc or shLIMIT cells were treated with IFNγ for 48 h. Surface expression of HLA-ABC was determined using flow cytometry (fluorescence-activated cell sorting (FACS)). Statistical analysis was performed using two-sided *t*-tests. MFI, mean fluorescence intensity. **d–g**, YUMM1.7 (**d**,**e**) or CT26 (**f**,**g**) cells carrying shFluc or shLimit were treated with IFNγ. RNA levels of Limit were determined 24 h after treatment (**d**,**f**). Surface staining of MHC-I (H2-D$^b$or H2-D$^d$) was detected 48 h after treatment (**e**,**g**). Statistical analysis was performed using two-sided *t*-tests. **h**,**i**, A375 WT cells or A375 cells with a deleted *LIMIT* promoter were treated with IFNγ. Indicated combination of paired guide RNA (ac, ad, bc, and bd) was employed to generate LIMIT promote deletion. RNA levels of LIMIT were determined 24 h after treatment (**h**). Surface expression of HLA-ABC was determined 48 h after treatment (**i**). Statistical analysis was performed using two-sided *t*-tests. **j**,**k**, B16 cells were transfected with dCas9-VPR, together with non-targeting sgRNA (sgNT) or sgRNA targeting the promoter of *Limit* (sgLimit). RNA levels of Limit were determined 24 h after treatment (**j**). Surface expression of MHC-I (H2-D$^b$) or PD-L1 were determined 48 h after treatment (**k**). Statistical analysis was performed using two-sided *t*-tests. **l**, B16-OVA cells carrying shFluc or shB2m were manipulated with *Limit* CRISPRa (sgLimit) for 48 h. Surface expression of OVA-H2K$^b$ was determined using FACS analysis. Statistical analysis was performed using two-sided *t*-tests. **m**,**n**, B16-OVA cells were manipulated with *B2m* knockdown (shB2m) or *Limit* CRISPRa (sgLimit), and cocultured with OT-I cells at a ratio of 1:4. Cell death was measured by propidium iodide staining in CD45$^-$ tumour cells. Dot plots (**m**) and statistical results (**n**) are shown. Statistical analysis was performed using two-sided *t*-tests. All data are mean ± s.d. For **a**, **c**–**l** and **n**, $n = 3$ biological independent samples. Source data are available online.

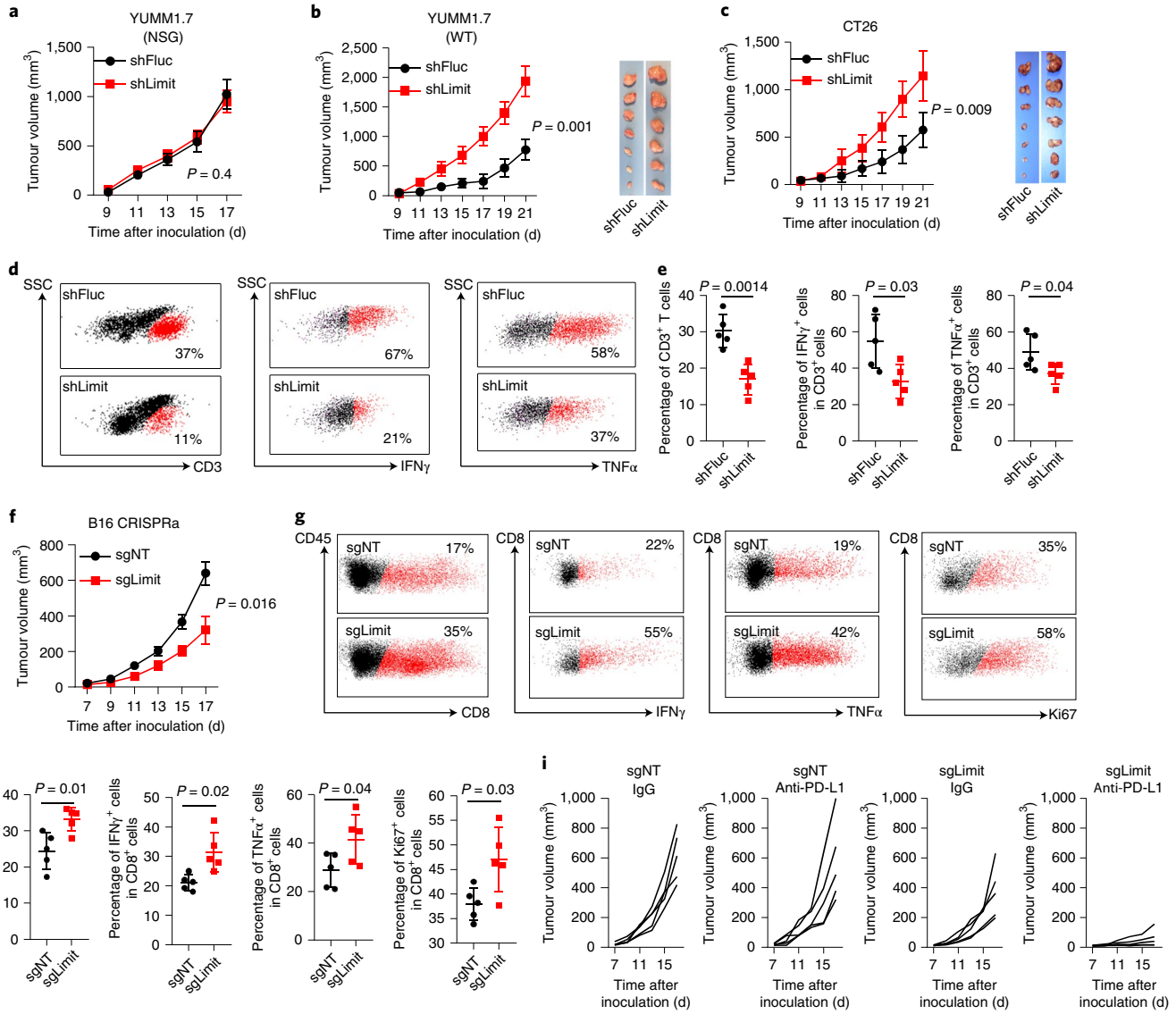


**Fig. 3 | LIMIT enhances anti-tumour immunity. a**, Tumour growth curve of YUMM1.7 shFluc or YUMM1.7 shLimit cells in NSG mice. $n = 5$ animals. Statistical analysis was performed using two-sided *t*-tests for the tumour volume at the end point. **b**, Tumour growth curve and tumour size of YUMM1.7 shFluc or YUMM1.7 shLimit cells inoculated in WT C57BL/6 mice. $n = 7$ (shFluc) or $n = 6$ (shLimit) animals. Statistical analysis was performed using two-sided *t*-tests for the tumour volume at the end point. **c**, Tumour growth curve of CT26 shFluc or CT26 shLimit cells in WT BALB/c mice. $n = 7$ animals. Statistical analysis was performed using two-sided *t*-tests for the tumour volume at the end point. **d**, Intratumoural $CD3^+$ T cells, $IFN\gamma^+$ T cells and $TNF\alpha^+$ T cells in YUMM1.7 shFluc or YUMM1.7 shLimit tumours. **e**, The percentages of intratumoural $CD3^+$ T cells (of $CD45^+$), $IFN\gamma^+$ T cells and $TNF\alpha^+$ T cells in YUMM1.7 shFluc or YUMM1.7 shLimit tumours. Statistical analysis was performed using two-sided *t*-tests. **f**, Tumour growth curve of B16 sgNT or B16 sgLimit (CRISPRa) cells in WT C57BL/6 mice. $n = 5$ animals. Statistical analysis was performed using two-sided *t*-tests. **g**, Intratumoural T-cell population and activation in B16 sgNT or B16 sgLimit tumours. **h**, Intratumoural T-cell population or activation in B16 sgNT or B16 sgLimit tumours. Statistical analysis was performed using two-sided *t*-tests. **i**, Tumour growth curve of B16 sgNT cells and B16 sgLimit cells in response to IgG or anti-PD-L1 antibodies. $n = 5$ animals. All data are mean ± s.d. For **e** and **h**, $n = 5$ biological independent samples. Source data are available online.

LIMIT potentiates tumour immunity and sensitizes the tumour immunotherapy response.

## LIMIT *cis*-activates GBPs to boost MHC-I and tumour immunity

We next examined how LIMIT affects MHC-I and tumour immunity. lncRNAs can locally regulate expression of neighbouring genes[24]. LIMIT is localized closely to a gene cluster, GBPs, in both human and mouse genomes (Extended Data Fig. 2a,b). We asked whether LIMIT might regulate the expression of GBPs. Silencing LIMIT reduced the levels of precursor and mature GBP mRNAs (Fig. 4a), and GBP1–5 proteins (Fig. 4b) in human A375 cells in response to IFNγ treatment. The data suggest that LIMIT may promote the transcription of GBPs in *cis*. In support of this possibility, silencing *Limit* also diminished *Gbp2* expression in mouse YUMM1.7 and CT26 cells (Extended Data Fig. 6a,b). Furthermore, CRISPR activation of *Limit* induced the expression of *Gbp2* in B16 cells (Fig. 4c). To test whether LIMIT could *trans*-regulate GBPs, we forced expression of *LIMIT* cDNA in A375 cells. We found that GBP1 and multiple immune factors (including IRF1, HLA-ABC, and PD-L1) were unaltered by *LIMIT* overexpression (Extended Data Fig. 6c). Thus, LIMIT is a *cis*-acting lncRNA that is capable of inducing GBP expression.

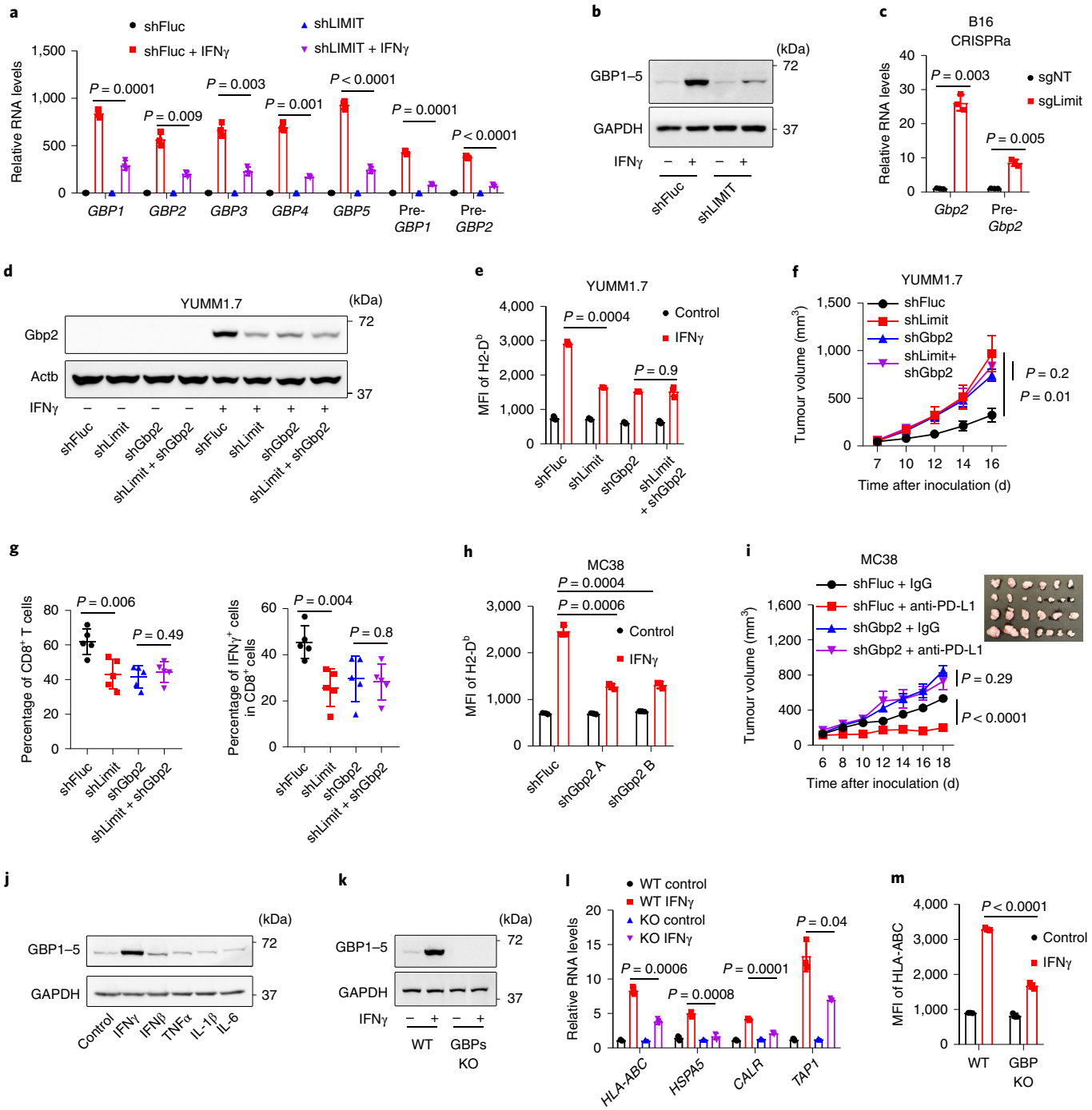


**Fig. 4 | LIMIT *cis*-activates GBPs to boost MHC-I and tumour immunity. a**,**b**, A375 shFluc or shLIMIT cells were treated with IFNγ for 24 h. RNA (**a**) or protein (**b**) levels of GBPs were determined. Statistical analysis was performed using two-sided *t*-tests. One out of three blots is shown. **c**, B16 cells were manipulated with *Limit* CRISPRa for 24 h. *Gbp2* precursor and mature RNAs were determined. Statistical analysis was performed using two-sided *t*-tests. **d**,**e**, YUMM1.7 shFluc, shLimit, shGbp2 or shLimit + shGbp2 cells were treated with IFNγ. Gbp2 protein was detected 24 h after treatment (**d**). Surface expression of MHC-I (H2-D$^b$) was measured 48 h after treatment (**e**). One out of two blots is shown. Statistical analysis was performed using two-sided *t*-tests. **f**, Tumour growth curves of YUMM1.7 shFluc, shLimit, shGbp2 or shLimit + shGbp2 cells inoculated in C57BL/6 mice. $n = 5$ animals. Statistical analysis was performed using two-sided *t*-tests for the tumour volume at the end point. **g**, The percentages of intratumoural CD8$^+$ T cells or IFNγ$^+$CD8$^+$ T cells in YUMM1.7 tumours carrying shFluc, shLimit, shGbp2 or shLimit + shGbp2. $n = 5$ animals. Statistical analysis was performed using two-sided *t*-tests. **h**, MC38 shFluc or shGbp2 cells were treated with IFNγ. Surface staining of H2-D$^b$ was determined 48 h after treatment. Statistical analysis was performed using two-sided *t*-tests. **i**, Tumour growth curves of MC38 shFluc and MC38 shGbp2 cells. Tumour-bearing mice were treated with IgG or anti-PD-L1 antibodies. $n = 6$ (shFluc) or $n = 7$ (shGbp2) animals. Statistical analysis was performed using two-sided *t*-tests for the tumour volume at the end point. **j**, A375 cells were treated with the indicated cytokines for 24 h. Protein levels of GBP1–5 were determined. One out of two experiments is shown. **k**–**m**, A375 WT or GBP1–5 KO cells were treated with IFNγ. GBP1–5 protein (**k**) and MHC-I-related gene transcripts (**l**) were determined 24 h after treatment. MHC-I surface expression (**m**) was determined 48 h after treatment. One out of three blots is shown. Statistical analysis was performed using two-sided *t*-tests. All data are mean ± s.d. For **a**, **c**, **e**, **h**, **l** and **m**, $n = 3$ biological independent samples. Source data are available online.

Among Gbp family members, Gbp2 is a predominant Gbp family member in mouse cells (Extended Data Fig. 6d). To test whether LIMIT may regulate MHC-I through GBPs, we established stable YUMM1.7 cells carrying shFluc, shLimit, shGbp2 or shLimit + shGbp2. We found that, in response to IFNγ stimulation, shLimit and shGbp2 led to a comparable decrease in *Gbp2* and MHC-I expression; simultaneously silencing *Limit* and *Gbp2* failed to additionally alter *Gbp2* and MHC-I expression (Fig. 4d,e). Moreover, we wondered whether GBP overexpression may rescue downregulated MHC-I expression in *Limit*-knockdown tumour cells. We forced expression of *GBP1* in shLIMIT A375 cells ($GBP1^{OE}$) and treated these cells with IFNγ. We observed that shLIMIT resulted in reduced MHC-I expression in control cells, but not in $GBP1^{OE}$ cells (Extended Data Fig. 6e). Expression of PD-L1 and IRF1 was not affected by shLIMIT or $GBP1^{OE}$ (Extended Data Fig. 6e,f). Thus, Limit may regulate MHC-I expression in a GBP-dependent manner. We next inoculated YUMM1.7 cells with *Limit* and/or *Gbp2* silencing in C57BL/6 mice. Silencing *Limit* and silencing GBPs similarly resulted in faster tumour growth compared with the control group, whereas simultaneously silencing LIMIT and GBPs did not further affect tumour progression (Fig. 4f). Furthermore, we detected a decrease in tumour-infiltrating T-cell numbers and activation in shLimit tumours, shGbp2 tumours and shLimit + shGbp2 tumours (Fig. 4g and Extended Data Fig. 6g). Together, LIMIT augments MHC-I expression and tumour immunity in a GBP-dependent manner.

GBPs are IFNγ-responsive genes in fibroblasts[25] and macrophages[26] in the context of host defence against pathogens. However, a role of GBPs in cancer immunity is unknown. Given that silencing GBPs reduced MHC-I expression and $CD8^+$ T-cell activation (Fig. 4g and Extended Data Fig. 6g), we hypothesized that GBPs might affect the efficacy of cancer immunotherapy. To test this hypothesis, we silenced *Gbp2* in MC38 cells, a tumour model that is sensitive to immunotherapy[23]. As expected, silencing *Gbp2* in MC38 cells reduced MHC-I expression after IFNγ treatment (Fig. 4h), and largely abrogated the efficacy of PD-L1 blockade (Fig. 4i). This, along with the aforementioned data, suggest that LIMIT and GBPs are involved in controlling cancer immunotherapy efficacy. In support of this possibility, clinical data analysis revealed that high levels of GBP expression are correlated with *LIMIT* and MHC-I expression and immunotherapy response (Extended Data Fig. 6h–j) in patients with melanoma[14–17]. Furthermore, levels of GBP expression were positively associated with patient survival (Extended Data Fig. 6k). To validate whether GBPs are IFNγ-responsive genes in cancer cells, we stimulated A375 cells with IFNγ and other cytokines. GBPs were induced by IFNγ, but minimally affected by other immune cytokines (Fig. 4j). We next used the CRISPR–Cas9 system to target the shared sequences among GBP1–5, and generated GBP1–5-KO A375 cells (Fig. 4k). We observed that IFNγ poorly stimulated MHC-I gene machinery transcripts (Fig. 4l) and surface HLA-ABC proteins in GBP KO A375 cells (Fig. 4m). Thus, LIMIT *cis*-activates GBPs to boost MHC-I machinery and tumour immunity.

## GBPs activate HSF1 to stimulate MHC-I and tumour immunity

To demonstrate how GBPs may regulate MHC-I expression and tumour immunity, we forced expression of GBPs in A375 cells. Interestingly, overexpression of GBPs increased human MHC-I expression as shown by quantitative PCR with reverse transcription (RT–qPCR; Fig. 5a), membrane surface staining (Fig. 5b) and western blotting (Fig. 5c). The data suggest that GBPs may activate MHC-I at the transcriptional level. Consistently, overexpression of *Gbp2* increased the expression of mouse MHC-I in YUMM1.7 and B16 cells (Fig. 5d).

To identify the transcription factor(s) that regulate MHC-I through GBPs in response to IFNγ, we performed bioinformatics prediction using PROMO[27]. We found that eight transcription factors were altered by IFNγ in A375 cells that may target *HLA-ABC*, *HSPA5*, *CALR* and *TAP1*. Besides several well-known factors, HSF1 activity was highly induced by IFNγ (Extended Data Fig. 7a). By processing chromatin immunoprecipitation coupled with sequencing (ChIP–seq) datasets in ENCODE[28], we found that both STAT1 and HSF1 were enriched at the promoters of MHC-I-associated genes with different binding patterns (Extended Data Fig. 7b). We performed a ChIP assay using anti-HSF1 antibodies in IFNγ-stimulated A375 cells. HSF1 was enriched at the promoters of *HLA-ABC*, *HSPA5*, *CALR* and *TAP1*, but not *HPRT1*, a negative control (Fig. 5e). The results suggest that HSF1 is a transcription factor for MHC-I. HSF1 is usually activated by proteostasis interruption[29]. To test whether activation of HSF1 enhances MHC-I expression, we treated A375 cells with a list of stressors[30]: heat shock, oxidative stress (Luperox), inhibitors of translation (puromycin), proteasome (MG-132) and chaperone (17-AAG). Interestingly, these stressors universally stimulated MHC-I expression, whereas KRIBB11, a HSF1 inhibitor, reduced this effect (Fig. 5f and Extended Data Fig. 7c). Thus, activation of HSF1 generally induces MHC-I expression.

We next questioned whether GBPs could activate HSF1. Forced expression of GBPs induced the luciferase activity of HSF1 reporter HSE–Luc (Fig. 5g), as well as the phosphorylation of HSF1 (Fig. 5h). This suggests that GBPs could activate HSF1. IFNγ failed to induce *HSPA5* expression in GBP-KO A375 cells (Fig. 5i). Thus, IFNγ activates HSF1 by inducing GBP expression. Furthermore, treatment with KRIBB11, an HSF1 inhibitor, abrogated the upregulation of MHC-I mediated by GBP1 overexpression (Fig. 5j). Thus, GBPs stimulate MHC-I expression in an HSF1-dependent manner.

To solidify the mechanistic relationship between GBPs and HSF1, we silenced *Gbp2* and/or *Hsf1* in MC38 cells (Fig. 5k). After IFNγ treatment, silencing of *Gbp2* or *Hsf1* alone diminished MHC-I expression, but simultaneously silencing *Gbp2* and *Hsf1* failed to additionally modulate MHC-I expression (Fig. 5l). To demonstrate the functional relevance of the interplay between GBPs and HSF1 in tumour immunity, we inoculated MC38 tumour cells expressing shFluc, shGbp2, shHSF1 or shGbp2 + shHSF1 into C57BL/6 mice. In comparison to shFluc controls, silencing *Gbp2* and silencing *Hsf1* comparably accelerated tumour growth (Fig. 5m) and diminished tumour-infiltrating T-cell numbers and activation (Fig. 5n and Extended Data Fig. 7d). Moreover, simultaneously silencing *Gbp2* and *Hsf1* failed to further affect tumour growth and tumour-infiltrating T cells (Fig. 5m,n and Extended Data Fig. 7d). Together, GBPs stimulate MHC-I expression and antitumour immunity by activating HSF1.

## The LIMIT–GBP–HSF1 axis drives MHC-I and tumour immunity

We next examined how GBPs activate HSF1 to alter MHC-I expression and tumour immunity. Under normal conditions, monomeric HSF1 is associated with and suppressed by chaperones, such as HSP90 (ref. [31]). Interruption of their interaction permits trimerization and accumulation of HSF1 in the nucleus, resulting in transcriptional activation of its target genes[32]. We hypothesized that GBPs may disturb the association between HSP90 and HSF1, resulting in HSF1 activation. To test this possibility, we treated A375 cells with IFNγ and performed co-IP using anti-HSP90 antibodies. We found that IFNγ-induced endogenous GBPs were associated with HSP90 (Fig. 6a). Furthermore, we transfected A375 cells with exogenous Flag–GBP1 and performed the co-IP experiment with Flag-antibody. HSP90 was detected in the IP product of Flag–GBP1-transfected cells, but not vector-transfected control cells (Fig. 6b). Immunofluorescence staining demonstrated that GBPs and HSP90 were largely colocalized in the cytoplasm (Fig. 6c). When we transfected HEK293T cells with increasing doses of *GBP1* plasmids, HSP90-associated HSF1 was reduced in a dose-dependent

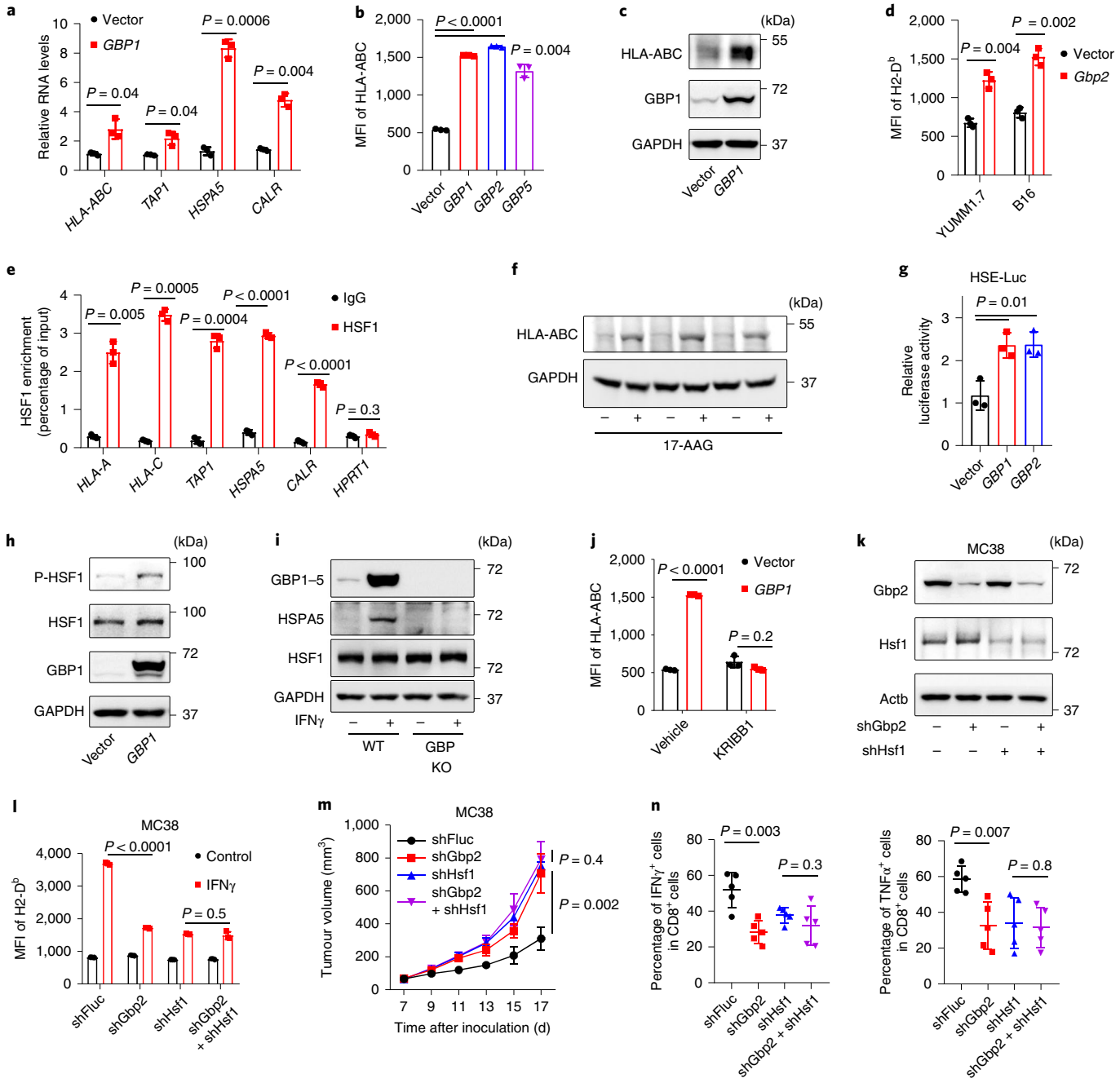


**Fig. 5 | GBPs activate HSF1 to stimulate MHC-I expression and tumour immunity. a–c**, A375 cells were forced to express GBPs. MHC-I RNA (**a**), surface expression (**b**) or total protein (**c**) levels were determined 24 h (**a**) or 48 h (**b**,**c**) afterwards. Statistical analysis was performed using two-sided *t*-tests. One out of two blots is shown. **d**, MHC-I surface expression in YUMM1.7 or B16 cells after *Gbp2* overexpression. Statistical analysis was performed using two-sided *t*-tests. **e**, HSF1 chromatin IP for the indicated gene promoters was performed in IFNγ-pretreated A375 cells. Statistical analysis was performed using two-sided *t*-tests. **f**, A375 cells were treated with 17-AAG to activate HSF1. Protein levels of HLA-ABC were determined 48 h after treatment. One out of two experiments is shown. **g**, A375 HSE-luc cells were forced to express GBPs. Luciferase activity was detected 48 h afterwards. Statistical analysis was performed using two-sided *t*-tests. **h**, A375 cells were forced to express *GBP1*. The levels of the indicated proteins were determined 12 h afterwards. One out of two experiments is shown. **i**, A375 WT or GBP KO cells were treated with IFNγ. The levels of the indicated proteins were determined 24 h afterwards. One out of two experiments is shown. **j**, A375 cells were forced to express *GBP1* and treated with KRIBB11. MHC-I surface expression was determined 48 h afterwards. Statistical analysis was performed using two-sided *t*-tests. **k**,**l**, MC38 shFluc, shGbp2, shHsf1 or shGbp2 + shHsf1 cells were treated with IFNγ. The levels of the indicated proteins (**k**) or MHC-I surface expression (**l**) were determined 48 h afterwards. One out of two experiments is shown. Statistical analysis was performed using two-sided *t*-tests. **m**, Tumour growth curves of MC38 shFluc, shGbp2, shHsf1 and shGbp2 + shHsf1 cells in C57BL/6 mice. $n = 5$ animals. Statistical analysis was performed using two-sided *t*-tests for the tumour volume at the end point. **n**, Percentages of intratumoural IFNγ$^+$CD8$^+$ T cells or TNFα$^+$CD8$^+$ T cells in MC38 tumours carrying shFluc, shGbp2, shHsf1 or shGbp2 + shHsf1. $n = 5$ biological independent samples. Statistical analysis was performed using two-sided *t*-tests. All data are mean ± s.d. For **a**, **b**, **d**, **e**, **g**, **j** and **l**, $n = 3$ biological independent samples. Source data are available online.

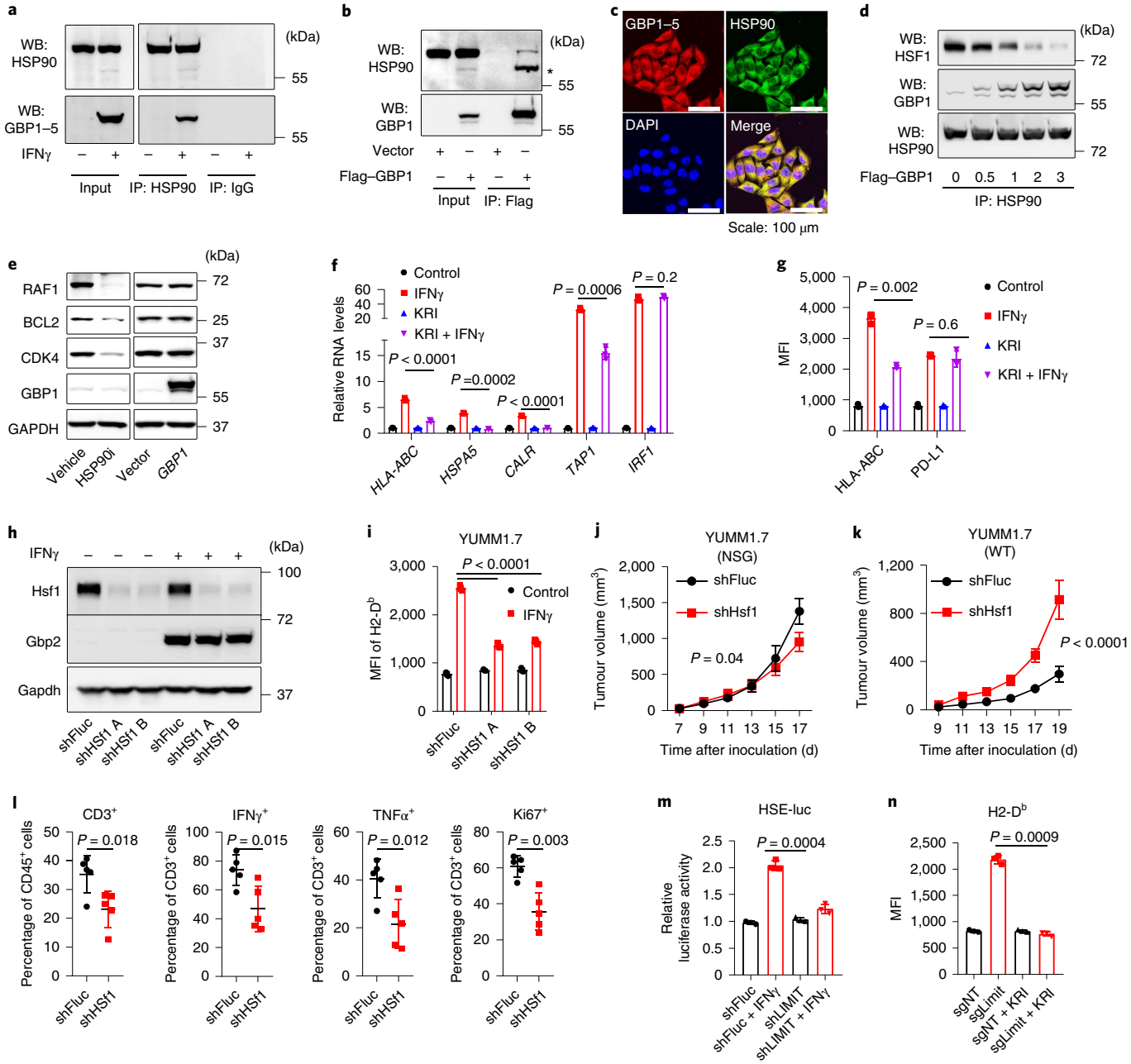


**Fig. 6 | The LIMIT–GBP–HSF1 axis drives MHC-I and tumour immunity. a**, Co-IP analysis of GBP1–5 using anti-HSP90 antibodies in IFNγ-pretreated A375 cells. One out of three experiments is shown. WB, western blot. **b**, Co-IP analysis of HSP90 using anti-Flag antibodies in A375 cells overexpressing Flag–GBP1. The asterisk indicates the band shift of HSP90 after GBP1 overexpression. One out of two experiments is shown. **c**, Immunofluorescence staining of GBP1 and HSP90 in IFNγ-pretreated A375 cells. One out of four images is shown. **d**, HEK293T cells were forced to express Flag-HSF1 and indicated amount (μg) of Flag-GBP1. Co-IP analysis of HSF1 or GBP1 with anti-HSP90 antibodies was performed 24 h afterwards. One out of two experiments is shown. **e**, A375 cells were treated with HSP90 inhibitor (HSP90i), or forced to express GBP1. The indicated proteins were detected 48 h afterwards. One out of two experiments is shown. **f**,**g**, A375 cells were treated with IFNγ and KRIBB11. RNA (**f**) or surface staining (**g**) levels of the indicated genes were determined 48 h afterwards. Statistical analysis was performed using two-sided *t*-tests. **h**,**i**, YUMM1.7 shFluc or shHsf1 cells were treated with IFNγ. Total protein (**h**) or surface expression (**i**) levels of the indicated genes were determined 48 h afterwards. One out of two experiments is shown. Statistical analysis was performed using two-sided *t*-tests. **j**,**k**, Tumour growth curves of YUMM1.7 shFluc or shHsf1 cells in NSG mice (**j**) or WT C57BL/6 mice (**k**). $n = 5$ (**j**) or $n = 6$ (**k**) mice. Statistical analysis was performed using two-sided *t*-tests for the tumour volume at the end point. **l**, Percentages of CD3$^+$, Ki67$^+$, IFNγ$^+$ and TNFα$^+$ T cells in YUMM1.7 shFluc or shHsf1 tumours. $n = 5$ biological independent samples. Statistical analysis was performed using two-sided *t*-tests. **m**, A375 shFluc or shLIMIT cells were transfected with HSE-LUC and PRL-SV40 overnight, and then treated with IFNγ for a further 48 h. HSF1 transcriptional activity is depicted as the relative luciferase activity. Statistical analysis was performed using two-sided *t*-tests. **n**, B16 cells were manipulated with *Limit* CRISPRa and treated with KRIBB11. Surface expression of MHC-I (H2-D$^b$) was determined 48 h afterwards. Statistical analysis was performed using two-sided *t*-tests. All data are mean ± s.d. For **f**, **g**, **i**, **m** and **n**, $n = 3$ biological independent samples. Source data are available online.

manner (Fig. 6d). The data suggest that GBPs interacted with HSP90 and this interaction disrupted the association between HSF1 and HSP90. HSP90 is a chaperone for multiple protein folding and stability, we questioned whether GBPs may alter the chaperone activity of HSP90. Although HSP90 inhibitor suppressed the expression of HSP90 client proteins (such as RAF1, BCL2 and CDK4)[33], overexpression of GBPs failed to do so (Fig. 6e). Thus, GBPs interact with HSP90, and release HSP90-associated HSF1, but do not alter HSP90 activity.

We next directly examined the role of HSF1 in MHC-I expression. We treated A375 cells with IFNγ in the presence of the HSF1 inhibitor KRIBB11. As expected, treatment with KRIBB11 reduced IFNγ-stimulated mRNA expression of MHC-I-related genes, including *HLA-ABC*, *TAP1*, *HSPA5* and *CALR*, but not *IRF1* (Fig. 6f). Interestingly, KRIBB11 reduced IFNγ-induced MHC-I expression, but had a minimal effect on PD-L1 expression (Fig. 6g). Thus, HSF1 can regulate IFNγ-induced MHC-I expression without altering the global IFNγ signalling.

To investigate whether HSF1-regulated MHC-I was functional, we cultured B16-OVA with OT-I cells in the presence of KRIBB11 and IFNγ. KRIBB11 inhibited IFNγ-induced expression of OVA-bound MHC-I (Extended Data Fig. 8a). Consistent with this, KRIBB11 also suppressed OT-I-cell-mediated cytotoxic effects on B16-OVA (Extended Data Fig. 8b). To extend our observations to additional tumours, we silenced *Hsf1* with shHsf1 in YUMM1.7 and CT26 cells. Silencing *Hsf1* resulted in a decrease in MHC-I expression in YUMM1.7 (Fig. 6h,i) and CT26 cells (Extended Data Fig. 8c) in response to IFNγ stimulation. In YUMM1.7 cells, silencing *Hsf1* failed to affect *Gbp2* expression in response to IFNγ (Fig. 6h), indicating that *Gbp2* is not an HSF1-target gene. In shHsf1 YUMM1.7 cells, KRIBB11 failed to suppress IFNγ-stimulated MHC-I expression (Extended Data Fig. 8d). The data suggest that HSF1 enhanced MHC-I expression in response to IFNγ, and *Hsf1* is the mechanistic target of KRIBB11 to regulate MHC-I.

Given that HSF1 affected MHC-I expression, we hypothesized that HSF1 regulated anti-tumour immunity in vivo. To test this hypothesis, we inoculated control and shHsf1 YUMM1.7 tumour cells into NSG and C57BL/6 mice. We observed that silencing *Hsf1* partially slowed down YUMM1.7 tumour progression in NSG mice (Fig. 6j), supporting that Hsf1 helped to maintain protein homeostasis and tumour progression in the immune-deficient model. However, silencing *Hsf1* substantially accelerated YUMM1.7 tumour growth in WT C57BL/6 mice (Fig. 6k). The data indicate that Hsf1 may surprisingly promote potent anti-tumour immunity in the immune competent model. In support of this, we detected a decrease in the percentages of tumour-infiltrating $CD3^+$, $Ki67^+$, $IFN\gamma^+$ and $TNF\alpha^+$ T cells (Fig. 6l and Extended Data Fig. 8e) in the shHsf1 YUMM1.7 tumours compared with the shFluc scramble controls. Furthermore, we inoculated shHsf1 CT26 cells into WT BALB/c mice. Again, silencing *Hsf1* resulted in enhanced CT26 tumour growth (Extended Data Fig. 8f). This was accompanied by a decrease in the percentages of tumour-infiltrating $CD3^+$, $Ki67^+$, $IFN\gamma^+$ and $TNF\alpha^+$ T cells (Extended Data Fig. 8g,h). Together, the data suggest that the GBP–HSF1 axis drives MHC-I expression and antitumour immunity.

To mechanistically connect HSF1 and LIMIT, we silenced *LIMIT* in A375 cells. Silencing LIMIT reduced the transcriptional activity of HSF1 in response to IFNγ, as determined by luciferase reporter assay (HSE-LUC) (Fig. 6m). The data suggest that LIMIT contributes to HSF1 activation in response to IFNγ. To test a potential involvement of HSF1 in the LIMIT-mediated induction of MHC-I, we stimulated LIMIT through CRISPR activation in B16 cells in the presence of KRIBB11. We observed that MHC-I upregulation, induced by LIMIT-activation, was abrogated by a HSF1 inhibitor (Fig. 6n). The data suggest that LIMIT boosts MHC-I expression in an HSF1-dependent manner.

Finally, we analysed a link between LIMIT, GBPs and HSF1 in the context of MHC-I expression, tumour immunity and immunotherapy in patients with cancer. Clinical analysis showed that HSF1-signalling genes were correlated with MHC-I expression, $CD8^+$ T-cell infiltration and patient survival (Extended Data Fig. 9a–c). In an immune checkpoint blockade study in patients with basal cell carcinoma[34], single-cell RNA-seq analysis revealed two tumour clusters; one tumour cluster was more sensitive to anti-PD-1 treatment as shown by a largely reduced tumour population (Extended Data Fig. 9d). Interestingly, this immune-checkpoint-sensitive tumour cluster expressed higher levels of HSF1-signalling genes as well as MHC-I gene machinery (Extended Data Fig. 9e). Moreover, in an immune checkpoint blockade study in patients with melanoma[35], proteomic analysis demonstrated that the protein expression of GBPs, HSF1 signalling genes and MHC-I were higher in clinical responders compared with those in non-responders (Extended Data Fig. 9f). Moreover, we observed a positive correlation between GBP1 and HSF1 signalling genes in human cancers (Extended Data Fig. 9g). The data support that the LIMIT–GBP–HSF1 axis may activate MHC-I expression and favour anti-tumour immunity (Extended Data Fig. 10).

## Discussion

Humans have 30,000–60,000 lncRNAs. However, the identities and biological functions of the vast majority of these potential lncRNAs remain poorly understood. In the cancer biology field, lncRNAs have been largely studied in the immune deficient model, leaving a knowledge gap of lncRNAs in the context of the immune system. A handful of lncRNAs are reported to affect immune cell function[36,37], cancer progression and chemotherapy efficacy[38,39]. However, whether specific lncRNAs are involved in antitumour immunity and immunotherapy response remains unanswered. Here we identified that LIMIT is an IFNγ-responsive lncRNA in both human and mouse cells. LIMIT can induce MHC-I and MHC-II expression, promoting T-cell-mediated tumour immune response and enhancing immunotherapy efficacy. Thus, LIMIT is a tumour immunogenic lncRNA.

The IFNγ signalling pathway has a key role in determining therapeutic response to cancer immunotherapy[40] by multiple mechanisms[19,20,41,42]. Genetic mutations in IFNγ signalling genes contribute to checkpoint blockade resistance in patients with cancer[43–48]. However, IFNγ signalling can induce inhibitory PD-L1 expression[49]. Thus, it is ideal to identify and target a key IFNγ signalling gene that selectively mediates anti-tumour immunity, rather than tumour immune evasion. In line with this notion, we demonstrate that LIMIT mediates MHC-I and MHC-II upregulation, but has no effect on PD-L1 expression in response to IFNγ. Thus, LIMIT may be uniquely positioned to be an immunogenic target for cancer immunotherapy.

Several strategies have been proposed to therapeutically target pathogenic lncRNAs[50]. However, how to elevate the levels of beneficial lncRNAs remains challenging. As *cis*-acting lncRNAs function locally, forced expression of these lncRNAs may be incapable of locating precisely[51]. Although *trans*-acting lncRNAs may function through specific secondary structures, overexpression of these lncRNAs may not be able to generate their natural structures due to missing appropriate RNA chaperones[52]. Using an RNA-guided CRISPR activation strategy[22], we directly activated LIMIT expression in tumour cells in preclinical models. RNA-guided CRISPR LIMIT activation can drive tumour MHC-I expression and potentiate checkpoint blockade therapy. Given that a loss of MHC-I and IFNγ gene signatures frequently occurs in human tumours, we suggest that CRISPR activation of beneficial lncRNAs, such as LIMIT, can rescue tumour MHC-I expression and be a potential therapeutic approach.

While searching for the mechanism by which LIMIT affects tumour immunity, we elucidated that LIMIT targets GBPs in an

in *cis* manner[24]. GBPs have a role in innate immunity[26,53,54]. Mice lacking the entire cluster of *Gbps* manifest a poor anti-*Toxoplasma gondii* response[55]. However, previously, the mechanistic connection between LIMIT and GBPs, and biological function of GBPs in tumour immunity and immunotherapy remained unclear. We have discovered that GBPs are required for IFNγ-induced tumour MHC-I expression, $CD8^+$ T-cell killing efficiency and effective checkpoint therapy. The data suggest that GBPs are potential target genes to boost tumour immunogenicity. We have unexpectedly uncovered that GBPs activate HSF1 to stimulate MHC-I and MHC-I related gene expression. HSF1 activation mediated by HSP90 inhibitors is correlated with tumour control in immunocompetent models[56,57]. However, despite multiple clinical trials with HSP90 inhibitors, none of the evaluated HSP90 inhibitors has been approved by the FDA for cancer therapy to date[58]. This disappointing fact raises the possibility that HSP90 inhibitors may be detrimental to tumour immunity. The toxicity of these HSP90 inhibitors may foster their destruction of several HSP90 client proteins, such as RAF1 and BCL2, which may be critical for effector T-cell proliferation and survival[59,60]. Given that GBPs interact with HSP90 and release HSP90-decoyed HSF1, but do not alter HSP90 activity, our data suggest that targeting GBPs may be a previously unappreciated and safe strategy to activate HSF1 for cancer immunotherapy.

In summary, we identify that LIMIT is a cancer immunogenic lncRNA. Our research suggests that targeting the LIMIT–GBP–HSF1 signalling axis can rescue expression and function of MHC-I, presenting a promising cancer immunotherapeutic approach.

## Online content

Any methods, additional references, Nature Research reporting summaries, source data, extended data, supplementary information, acknowledgements, peer review information; details of author contributions and competing interests; and statements of data and code availability are available at https://doi.org/10.1038/s41556-021-00672-3.

Received: 16 October 2020; Accepted: 31 March 2021;
Published online: 6 May 2021

## References

1. Zou, W., Wolchok, J. D. & Chen, L. PD-L1 (B7-H1) and PD-1 pathway blockade for cancer therapy: mechanisms, response biomarkers, and combinations. *Sci. Transl. Med.* **8**, 328rv324 (2016).
2. Schumacher, T. N. & Schreiber, R. D. Neoantigens in cancer immunotherapy. *Science* **348**, 69–74 (2015).
3. Garcia-Lora, A., Algarra, I. & Garrido, F. MHC class I antigens, immune surveillance, and tumor immune escape. *J. Cell. Physiol.* **195**, 346–355 (2003).
4. Festenstein, H. & Garrido, F. MHC antigens and malignancy. *Nature* **322**, 502–503 (1986).
5. Garrido, F., Aptsiauri, N., Doorduijn, E. M., Garcia Lora, A. M. & van Hall, T. The urgent need to recover MHC class I in cancers for effective immunotherapy. *Curr. Opin. Immunol.* **39**, 44–51 (2016).
6. Hon, C. C. et al. An atlas of human long non-coding RNAs with accurate 5′ ends. *Nature* **543**, 199–204 (2017).
7. Mercer, T. R., Dinger, M. E. & Mattick, J. S. Long non-coding RNAs: insights into functions. *Nat. Rev. Genet.* **10**, 155–159 (2009).
8. Ponting, C. P., Oliver, P. L. & Reik, W. Evolution and functions of long noncoding RNAs. *Cell* **136**, 629–641 (2009).
9. Wilusz, J. E., Sunwoo, H. & Spector, D. L. Long noncoding RNAs: functional surprises from the RNA world. *Genes Dev.* **23**, 1494–1504 (2009).
10. Kung, J. T., Colognori, D. & Lee, J. T. Long noncoding RNAs: past, present, and future. *Genetics* **193**, 651–669 (2013).
11. Flynn, R. A. & Chang, H. Y. Long noncoding RNAs in cell-fate programming and reprogramming. *Cell Stem Cell* **14**, 752–761 (2014).
12. Huarte, M. The emerging role of lncRNAs in cancer. *Nat. Med.* **21**, 1253–1261 (2015).
13. Frankish, A. et al. GENCODE reference annotation for the human and mouse genomes. *Nucleic Acids Res.* **47**, D766–D773 (2019).
14. Riaz, N. et al. Tumor and microenvironment evolution during immunotherapy with nivolumab. *Cell* **171**, 934–949 (2017).
15. Hugo, W. et al. Genomic and transcriptomic features of response to anti-PD-1 therapy in metastatic melanoma. *Cell* **168**, 542 (2017).
16. Van Allen, E. M. et al. Genomic correlates of response to CTLA-4 blockade in metastatic melanoma. *Science* **350**, 207–211 (2015).
17. Nathanson, T. et al. Somatic mutations and neoepitope homology in melanomas treated with CTLA-4 blockade. *Cancer Immunol. Res* **5**, 84–91 (2017).
18. Sui, J. et al. Systematic analyses of a novel lncRNA-associated signature as the prognostic biomarker for hepatocellular carcinoma. *Cancer Med*. https://doi.org/10.1002/cam4.1541 (2018).
19. Kaplan, D. H. et al. Demonstration of an interferon γ-dependent tumor surveillance system in immunocompetent mice. *Proc. Natl Acad. Sci. USA* **95**, 7556–7561 (1998).
20. Fruh, K. & Yang, Y. Antigen presentation by MHC class I and its regulation by interferon γ. *Curr. Opin. Immunol.* **11**, 76–81 (1999).
21. Dong, H. et al. Tumor-associated B7-H1 promotes T-cell apoptosis: a potential mechanism of immune evasion. *Nat. Med.* **8**, 793–800 (2002).
22. Perez-Pinera, P. et al. RNA-guided gene activation by CRISPR-Cas9-based transcription factors. *Nat. Methods* **10**, 973–976 (2013).
23. Lin, H. et al. Host expression of PD-L1 determines efficacy of PD-L1 pathway blockade-mediated tumor regression. *J. Clin. Invest.* **128**, 805–815 (2018).
24. Sun, Q., Hao, Q. & Prasanth, K. V. Nuclear long noncoding RNAs: key regulators of gene expression. *Trends Genet.* **34**, 142–157 (2018).
25. Cheng, Y. S., Colonno, R. J. & Yin, F. H. Interferon induction of fibroblast proteins with guanylate binding activity. *J. Biol. Chem.* **258**, 7746–7750 (1983).
26. Kim, B. H. et al. Interferon-induced guanylate-binding proteins in inflammasome activation and host defense. *Nat. Immunol.* **17**, 481–489 (2016).
27. Messeguer, X. et al. PROMO: detection of known transcription regulatory elements using species-tailored searches. *Bioinformatics* **18**, 333–334 (2002).
28. Consortium, E. P. An integrated encyclopedia of DNA elements in the human genome. *Nature* **489**, 57–74 (2012).
29. Dai, C. & Sampson, S. B. HSF1: guardian of proteostasis in cancer. *Trends Cell Biol.* **26**, 17–28 (2016).
30. West, J. D., Wang, Y. & Morano, K. A. Small molecule activators of the heat shock response: chemical properties, molecular targets, and therapeutic promise. *Chem. Res. Toxicol.* **25**, 2036–2053 (2012).
31. Zou, J., Guo, Y., Guettouche, T., Smith, D. F. & Voellmy, R. Repression of heat shock transcription factor HSF1 activation by HSP90 (HSP90 complex) that forms a stress-sensitive complex with HSF1. *Cell* **94**, 471–480 (1998).
32. Dayalan Naidu, S. & Dinkova-Kostova, A. T. Regulation of the mammalian heat shock factor 1. *FEBS J.* **284**, 1606–1627 (2017).
33. Whitesell, L. & Lindquist, S. L. HSP90 and the chaperoning of cancer. *Nat. Rev. Cancer* **5**, 761–772 (2005).
34. Yost, K. E. et al. Clonal replacement of tumor-specific T cells following PD-1 blockade. *Nat. Med.* **25**, 1251–1259 (2019).
35. Harel, M. et al. Proteomics of melanoma response to immunotherapy reveals mitochondrial dependence. *Cell* **179**, 236–250 (2019).
36. Heward, J. A. & Lindsay, M. A. Long non-coding RNAs in the regulation of the immune response. *Trends Immunol.* **35**, 408–419 (2014).
37. Flores-Concha, M. & Onate, A. A. Long non-coding RNAs in the regulation of the immune response and trained immunity. *Front. Genet.* **11**, 718 (2020).
38. Schmitt, A. M. & Chang, H. Y. Long noncoding RNAs in cancer pathways. *Cancer Cell* **29**, 452–463 (2016).
39. Sun, T. T. et al. LncRNA GClnc1 promotes gastric carcinogenesis and may act as a modular scaffold of WDR5 and KAT2A complexes to specify the histone modification pattern. *Cancer Discov.* **6**, 784–801 (2016).
40. Sharma, P., Hu-Lieskovan, S., Wargo, J. A. & Ribas, A. Primary, adaptive, and acquired resistance to cancer immunotherapy. *Cell* **168**, 707–723 (2017).
41. Peng, D. et al. Epigenetic silencing of TH1-type chemokines shapes tumour immunity and immunotherapy. *Nature* **527**, 249–253 (2015).
42. Wang, W. et al. $CD8^+$ T cells regulate tumour ferroptosis during cancer immunotherapy. *Nature* **569**, 270–274 (2019).
43. Gao, J. et al. Loss of IFN-γ pathway genes in tumor cells as a mechanism of resistance to anti-CTLA-4 therapy. *Cell* **167**, 397–404 (2016).
44. Zaretsky, J. M. et al. Mutations associated with acquired resistance to PD-1 blockade in melanoma. *N. Engl. J. Med.* **375**, 819–829 (2016).
45. Manguso, R. T. et al. In vivo CRISPR screening identifies *Ptpn2* as a cancer immunotherapy target. *Nature* **547**, 413–418 (2017).
46. Shin, D. S. et al. Primary resistance to PD-1 blockade mediated by JAK1/2 mutations. *Cancer Discov.* **7**, 188–201 (2017).
47. Sucker, A. et al. Acquired IFNγ resistance impairs anti-tumor immunity and gives rise to T-cell-resistant melanoma lesions. *Nat. Commun.* **8**, 15440 (2017).
48. Li, J. et al. Epigenetic driver mutations in ARID1A shape cancer immune phenotype and immunotherapy. *J. Clin. Invest.* https://doi.org/10.1172/JCI134402 (2020).

49. Benci, J. L. et al. Tumor interferon signaling regulates a multigenic resistance program to immune checkpoint blockade. *Cell* **167**, 1540–1554 (2016).
50. Arun, G., Diermeier, S. D. & Spector, D. L. Therapeutic targeting of long non-coding RNAs in cancer. *Trends Mol. Med.* **24**, 257–277 (2018).
51. Gil, N. & Ulitsky, I. Regulation of gene expression by cis-acting long non-coding RNAs. *Nat. Rev. Genet.* **21**, 102–117 (2020).
52. Jones, A. N. & Sattler, M. Challenges and perspectives for structural biology of lncRNAs-the example of the Xist lncRNA A-repeats. *J. Mol. Cell. Biol.* **11**, 845–859 (2019).
53. Shenoy, A. R. et al. GBP5 promotes NLRP3 inflammasome assembly and immunity in mammals. *Science* **336**, 481–485 (2012).
54. Tretina, K., Park, E. S., Maminska, A. & MacMicking, J. D. Interferon-induced guanylate-binding proteins: guardians of host defense in health and disease. *J. Exp. Med.* **216**, 482–500 (2019).
55. Yamamoto, M. et al. A cluster of interferon-γ-inducible p65 GTPases plays a critical role in host defense against *Toxoplasma gondii*. *Immunity* **37**, 302–313 (2012).
56. Mbofung, R. M. et al. HSP90 inhibition enhances cancer immunotherapy by upregulating interferon response genes. *Nat. Commun.* **8**, 451 (2017).
57. Proia, D. A. & Kaufmann, G. F. Targeting heat-shock protein 90 (HSP90) as a complementary strategy to immune checkpoint blockade for cancer therapy. *Cancer Immunol. Res.* **3**, 583–589 (2015).
58. Yuno, A. et al. Clinical evaluation and biomarker profiling of Hsp90 inhibitors. *Methods Mol. Biol.* **1709**, 423–441 (2018).
59. Charo, J. et al. Bcl-2 overexpression enhances tumor-specific T-cell survival. *Cancer Res.* **65**, 2001–2008 (2005).
60. Owaki, H. et al. Raf-1 is required for T cell IL2 production. *EMBO J.* **12**, 4367–4373 (1993).

## Methods

**Animal experiments.** Female NSG (NOD.Cg-*Prkdc*$^{scid}$ *Il2rg*$^{tm1Wjl}$/SzJ, Stock, 005557), C57BL/6 (C57BL/6J, Stock, 000664), BALB/c (BALB/cJ, Stock, 000651) and OT-1 (C57BL/6-Tg(TcraTcrb)1100Mjb/J, Stock, 003831) mice (aged 6–8 weeks) were obtained from the Jackson Laboratory. All mice were maintained under pathogen-free conditions. The animal room has a controlled temperature (18–23 °C), humidity (40–60%) and a 12 h–12 h light–dark cycle. YUMM1.7 ($1\times10^5$), CT26 ($1\times10^5$), MC38 ($2.5\times10^6$) and B16 ($1\times10^5$) cells were subcutaneously injected into the right flank of the mice. For anti-PD-L1 treatment in the MC38 model, 5 mg kg$^{-1}$ anti-PD-L1 antibodies (InVivoMAb, 10F.9G2) and control antibodies (InVivoMAb, LTF-2) were intraperitoneally administered on days 6, 9 and 12 after tumour inoculation. For anti-PD-L1 treatment in the B16 model, 5 mg kg$^{-1}$ anti-PD-L1 antibodies (InVivoMAb, 10F.9G2) and control antibodies (InVivoMAb, LTF-2) were intraperitoneally administered on days 0, 3, 6, 9, 12 and 15 after tumour inoculation. Tumour diameters were measured using callipers. Tumour volume was calculated by length × width × width/2. Animal studies were conducted under the approval of the Institutional Animal Care and Use Committee at the University of Michigan (PRO00008278). The study is compliant with all of the relevant ethical regulations regarding animal research. In none of the experiments did xenograft tumour size surpass 2 cm in any dimensions, and no animal had severe abdominal distension (≥10% original body weight increase). Sample size was chosen on the basis of preliminary data. After tumour inoculation, mice were randomized and assigned to different groups for treatment.

**Reagents.** KRIBB11 and 17-AAG were purchased from Cayman Chemical. MG-132, and puromycin and Luperox were obtained from Sigma-Aldrich. Recombinant human IFNγ (285-IF), IFNβ (8499-IF), TNFα (210-TA), IL-1β (201-LB), IL-6 (206-IL) and mouse IFNγ (485-MI) were obtained from R&D.

**Plasmids.** To generate HSE-LUC, DNA sequences corresponding to heat shock elements (HSE) were synthesized, annealed and ligated into PGL3-basic (Promega) plasmid. Flag–HSF1 was a gift from S. Calderwood (Addgene, 32537). For forced expression of human *GBP1*, *GBP2* and *GBP5*, and mouse *Gbp2*, the respective coding sequences were PCR-amplified from the cDNA generated from IFNγ-pretreated A375 cells or B16 cells, and subsequently inserted into PCI-Flag plasmid. PCI-Flag plasmid was prepared by inserting the Kozak sequence plus Flag tag plus 5× glycine sequence into the PCI-neo (Promega) plasmid between NheI and XhoI. To knockdown human *LIMIT* and mouse *Limit*, shRNAs were designed and inserted into the PLKO.1 plasmid (Addgene, 10879). The shRNA targeting firefly luciferase (shFluc) was used as a negative control. To target the promoter region of *Limit* for CRISPR activation, sgRNAs (sgLimit) were designed and inserted into the phU6-sgRNA plasmid (Addgene, 53188). The non-targeting sgRNA (sgNT) was used as a negative control. To delete the STAT1/IRF1-binding sites in the *LIMIT* promoter, paired sgRNAs (psgLIMIT) were designed and inserted into the PX459 plasmid (Addgene, 48139). To knockdown mouse *Hsf1* and *Gbp2*, shRNAs were designed and inserted into the PLKO.1 plasmid (Addgene, 10879). To knock out *GBP1–5*, sgRNA was designed and inserted into the PX459 plasmid (Addgene, 48139). A list of the target sequences is provided in Supplementary Table 7. A list of the primer sequences is provided in Supplementary Table 8.

**Cell culture.** Human melanoma cell line A375 (CRL-1619), mouse melanoma cell lines, B16-F0 (CRL-6322) and YUMM1.7 (CRL-3362) cells, mouse colon cancer cell line CT26 (CRL-2638) and HEK293T cells (CRL-3216) were purchased from the American Type Culture Collection. The mouse colon cancer cell line MC38 was used previously in the Zou laboratory[23,48]. B16-OVA cells were established as previously reported[42]. A375 *STAT1*-KO, A375 *GBP1–5*-KO and A375 *LIMIT*-promoter-deletion cell lines were generated in this study. All cell lines were tested for mycoplasma contamination routinely and confirmed to be negative for mycoplasma. Cells were cultured in RMPI medium (Gibco, 11875) supplemented with 10% FBS, with the exception of A375 and HEK293T cells; the latter two lines were cultured in DMEM (Gibco, 11965) supplemented with 10% FBS. All cells were maintained at 37 °C under 5% $CO_2$. For heat shock, cells were placed into an incubator at 43 °C under 5% $CO_2$ for 2 h. To generate knockdown cell lines, lentiviral particles were produced by transfection of PLKO.1 shRNA plasmid with psPAX2 (Addgene, 12260) and pMD2.G (Addgene, 12259) (4:3:1) into HEK293T cells, and subsequently transduced into tumour cells with polybrene (Sigma-Aldrich, 8 μg ml$^{-1}$) overnight. Next, 48 h after transfection, cells were selected with puromycin (1–2 μg ml$^{-1}$) for an additional 2 weeks. To establish knockout cell lines, PX459-sgRNA plasmids were transfected into tumour cells for 2 d and selected by puromycin (1–2 μg ml$^{-1}$) for an additional 2 d. The cells were then serially diluted and seeded into 96-well plates. After 2–3 weeks, single-cell colonies were dissociated and replated into six-well plates. After cell confluency, half of the cells were collected and validated for knockout efficiency using western blotting. To apply the CRISPR activation system to activate mouse *Limit*, phU6-sgRNAs were transfected together with SP-dCas9-VPR (Addgene, 63798) into B16 cells. All transfections were conducted using Lipofectamine 2000 (Thermo Fisher Scientific) at a ratio of 1 μg plasmid:2 μl transfection regent. The transfection dosage was determined by titration.

**Luciferase activity assay.** A375 cells were transfected with HSE-LUC and PRL-SV40P (Addgene, 27163) for 24 h, together with PCI-neo (vector) or *GBP1* or *GBP2* for 48 h. A375 shFluc or A375 shLIMIT cells were transfected with HSE-LUC and PRL-SV40P (Addgene, 27163) for 24 h, and then treated with IFNγ for an additional 48 h. Luciferase activity for firefly luciferase (HSE-LUC) and *Renilla* luciferase (PRL-SV40P) were measured using the Dual-Luciferase Reporter Assay System (Promega). Relative firefly luciferase activity was normalized to *Renilla* luciferase activity.

**Surface staining and flow cytometry analysis (FACS).** Cells were trypsinized and washed with MACS buffer (PBS, 2%FBS, 1 mM EDTA). Surface staining was performed by adding the following antibodies to the cell suspension in 50 μl MACS buffer: anti-HLA-ABC (G46-2.6, BD Biosciences), anti-H2-D$^b$ (KH95, BD Biosciences), anti-H2-D$^d$ (34-2-12, BD Biosciences), anti-OVA–H2-K$^b$ (eBio25-D1.16, eBioscience) and anti-PD-L1 (MIH1, BD Biosciences) antibodies. After incubating for 30 min, cells were washed with MACS buffer and analysed using the BD Fortessa flow cytometer.

**qPCR analysis.** Total RNA was isolated from cells by column purification (Direct-zol RNA Miniprep Kit, Zymo Research) with DNase treatment. cDNA was synthesized using the RevertAid First Strand cDNA Synthesis Kit (Thermo Fisher Scientific) with random hexamer primers. qPCR was performed on cDNA using the Fast SYBR Green Master Mix (Thermo Fisher Scientific) on a StepOnePlus Real-Time PCR System (Thermo Fisher Scientific). Gene expression was quantified using the primers listed in Supplementary Table 8. Fold changes in mRNA expression were calculated using the $\Delta\Delta C_t$ method using *ACTB* as an endogenous control. Results are expressed as fold change by normalizing to the controls.

**Northern blotting.** Northern blot analysis was performed with 10 μg of total RNAs prepared from IFNγ-, IFNβ- and TNFα-pretreated A375 cells. RNAs were resolved by denaturing agarose gel electrophoresis (Ambion) and transferred to Hybond-XL membranes (GE Healthcare). LIMIT was detected using digoxin-labelled DNA probes with the DIG Northern Starter Kit (Roche). A list of the probe sequences targeting LIMIT is provided in Supplementary Table 7.

**RACE.** RACE was performed to identify the cDNA ends of human *LIMIT* or mouse *Limit* using the SMARTer RACE cDNA Amplification Kit (Clontech). A list of the primers for RACE is provided in Supplementary Table 8.

**Clone of full-length *LIMIT*.** After obtaining the cDNA end sequences, full-length *LIMIT* was PCR amplified and inserted into PCI-neo plasmid between XhoI and NotI. A list of the cloning primers for human *LIMIT* and mouse *Limit* is provided in Supplementary Table 8.

**Cell fractionation for RT–PCR.** IFNγ-pretreated A375 cells were collected from 15 cm plates by scraping and were washed once with cold PBS. Cells were pelleted by centrifugation at 700*g* for 5 min and lysed with hypotonic lysis buffer (10 mM Tris (pH 7.5), 10 mM NaCl, 3 mM $MgCl_2$, 0.3% (v/v) NP-40, 10% (v/v) glycerol) to collect the cytoplasmic fraction. Cytoplasmic RNA was obtained by ethanol precipitation overnight at −20 °C, followed by re-extraction using TRIZOL reagent. The remaining nuclear pellet was washed three times with the hypotonic lysis buffer, followed by extraction with TRIZOL reagent according to the manufacturer's instructions. RNAs isolated from nuclear or cytoplasmic fractions were reverse-transcribed, and RT–PCR was performed for *LIMIT* using the indicated primers. Unspliced and mature *ACTB* was used as controls for nuclear or cytoplasmic RNA, respectively. A list of the primers for *ACTB* is provided in Supplementary Table 8.

**Western blot analysis.** Cells were washed in cold PBS and lysed in 1× RIPA lysis buffer (Pierce) with 1× protease inhibitor (Pierce). Lysates were incubated on ice for 10 min and cleared by centrifugation at 15,000*g* for 15 min. Protein concentration was quantified using a BCA protein assay kit (Thermo Fisher Scientific). Protein (30 μg) was mixed with sample buffer (Thermo Fisher Scientific) with β-ME and denatured at 95 °C for 5 min. The sample was separated by SDS–PAGE and transferred to a nitrocellulose membrane (Bio-Rad). Membranes were blocked with 5% w/v non-fat dry milk and incubated with primary antibodies overnight at 4 °C and HRP-conjugated secondary antibodies (CST) for 1 h at room temperature. Signal was detected using Clarity and Clarity Max Western ECL Blotting Substrates (Bio-Rad) and captured using the ChemiDoc Imaging System (Bio-Rad). Antibodies were as follows: anti-human GBP1–5 (Santa Cruz, 166960, 1:500), anti-HSF1 (CST, 12972, 1:1,000), anti-phosphorylated-HSF1 (Abcam, 76076, 1:1,000), anti-GBP1 (Proteintech, 15303, 1:1,000), anti-Gbp2 (Proteintech, 11854, 1:1,000), anti-HSP90 (CST, 4877, 1:1,000), anti-HSPA5 (CST, 3177, 1:1,000), anti-STAT1 (CST, 9172, 1:1,000), anti-phosphorylated-STAT1 (CST, 9167, 1:1,000), anti-RAF1 (CST, 9422, 1:1,000), anti-BCL2 (CST, 2870, 1:1,000), anti-CDK4 (CST, 12790, 1:1,000) and anti-GAPDH (Proteintech, 60004, 1:5,000). For human MHC-I western blot analysis, total cell lysates were denatured in the sample buffer without β-ME (non-reducing) to maintain the disulfide bridges and the conformation of the proteins to be detected by anti-HLA-ABC antibodies (W6/32, Novus Biologicals, 64775, 1:1,000).

**Co-IP analysis.** Cells were collected with IP lysis buffer (Pierce, 87787) plus protease inhibitor. Protein concentration was determined using the BCA protein assay kit. Protein samples (200–500 µg) were added to 1–3 µg primary antibodies (anti-HSP90 (Proteintech, 13171) or anti-HSF1 (CST, 12972)), and incubated with gentle rocking at 4 °C overnight. Samples were then further incubated with 20 µl Protein A/G PLUS-Agarose (Santa Cruz, sc-2003) for 2 h at 4 °C, and centrifuged at 7,500*g* for 30 s at 4 °C. Cell pellets were washed four times with IP lysis buffer, resuspended with 40 µl 2× sample buffer with β-ME, and heated for 5 min at 95 °C. The denatured protein samples were analysed using western blotting. For Flag IP, cell lysates were incubated with 20 µl EZview Red ANTI-FLAG M2 Affinity Gel (Sigma-Aldrich), and washed, denatured and analysed as described above.

**Immunofluorescence staining.** A375 cells mounted onto coverslips were treated with IFNγ for 24 h. After washing twice with PBS, cells were fixed with 4% PFA for 15 min and washed twice with PBS for 5 min each. The cells were next permeabilized with 0.5% Triton X-100 in PBS for 10 min and rinsed twice with PBS for 5 min each. Antigens were blocked with 10% normal goal serum in PBS for 30 min. Primary antibodies were then added at 1:50 dilutions of mouse anti-human GBP1–5 antibodies (Santa Cruz, 166960) or rabbit anti-human HSP90 antibodies (CST, 4877), and incubated at 4 °C overnight. The cells were then washed and incubated with 1:500 dilutions of Qdot 605-labelled secondary goat anti-mouse antibodies (Thermo Fisher Scientific, Q11002) or AF488-labelled secondary goat anti-rabbit antibodies (Thermo Fisher Scientific, A11034), and then mounted onto glass slides using ProLong Gold reagent containing DAPI. Confocal fluorescence images were collected using a ×63 oil-immersion objective (Leica SP5 Inverted 2-Photon FLIM confocal).

**ChIP analysis.** ChIPs were performed using cross-linked chromatin from IFNγ-treated A375 cells and either anti-HSF1 antibodies (CST, 12972) or normal rabbit IgG (CST, 2729), using the Simple ChIP Plus Enzymatic Chromatin IP Kit (Magnetic Beads) (CST, 9005). The enriched DNA was quantified by qPCR using the primers listed in Supplementary Table 8. The amount of immunoprecipitated DNA in each sample is represented as the signal relative to total amount of input chromatin, which is equivalent to 1.

**OT-I cell isolation and coculture with OVA$^+$ tumour cells.** C57BL/6-Tg(TcraTcrb) 1100Mjb/J (OT-I) mice (JAX stock, 003831) were purchased from the Jackson Laboratory. The spleen was homogenized, and single cells were suspended in 2 ml red blood cell lysis buffer (Sigma-Aldrich) for 1 min. The splenocytes were pelleted, washed and resuspended at $2\times10^6$ cells per ml in RPMI culture medium containing 1 µg ml$^{-1}$ OVA257-264 peptide, 5 µg ml$^{-1}$ mouse recombinant IL-2 and 40 µM 2-mercaptoethanol. The cells were incubated at 37 °C for 5 d. To set up the coculture of OT-I and OVA$^+$ tumour cells, splenocytes were collected after activation for 5 d. OT-I cells were purified using the EasySep mouse CD8$^+$ T Cell Isolation Kit (Stemcell). B16-OVA cells were seeded overnight. OT-I cells were then added into the culture at different ratios. All cells were collected by trypsinization and analysed using flow cytometry (FACS).

**Bone-marrow-derived dendritic cells and macrophages.** Bone marrow was isolated from C57BL/6 mouse femurs and cultured in RPMI 1640 complete medium with 20 ng ml$^{-1}$ GM-CSF (R&D). Cells were incubated at 37 °C under 5% $CO_2$. An additional 10 ml medium with 20 ng ml$^{-1}$ GM-CSF was added at day 3. On day 7, non-adherent and loosely adherent cells in the culture supernatant were collected by gentle washing with PBS, and considered to be bone-marrow-derived dendritic cells. The adherent cells were considered to be bone-marrow-derived macrophages.

**Intratumoural immune cell profiling.** To quantify intratumoural T cells and T-cell effector cytokine expression, single-cell suspensions were prepared from fresh tumour tissues by physically passing them through 100 µm cell strainers. Immune cells were enriched by density gradient centrifugation. For cytokine staining, intratumoural immune cells were incubated in RPMI culture medium containing PMA (5 ng ml$^{-1}$), ionomycin (500 ng ml$^{-1}$), brefeldin A (1:1,000) and monensin (1:1,000) at 37 °C for 4 h. Two to three microlitres of anti-CD45 (30-F11, BD Biosciences), anti-CD90 (53-2.1, BD Biosciences), anti-CD3 (145-2C11, BD Biosciences), anti-CD4 (RM4-5, BD Biosciences) and anti-CD8 (53-6.7, BD Biosciences) antibodies were added for 20 min for surface staining. The cells were then washed and resuspended in 1 ml of freshly prepared Fix/Perm solution (BD Biosciences) at 4 °C overnight. After being washed with Perm/Wash buffer (BD Biosciences), the cells were stained with 2–3 µl anti-Ki67 (B56, BD Biosciences), anti-TNF (MP6-XT22, BD Biosciences) and anti-IFNγ (XMG1.2, BD Biosciences) antibodies for 30 min, washed and fixed in 4% formaldehyde (Sigma-Aldrich). All of the samples were read using the LSR Fortessa cytometer and analysed using FACS DIVA v.8.0 (BD Biosciences).

**Signature score computation.** We used normalized expression of genes to define the following signatures: CD8$^+$ T-cell infiltration (*CD8A*, *CD8B*, *PRF1* and *GZMB*), MHC-I expression (*HLA-A*, *HLA-B* and *HLA-C*) and HSF1 signalling (*HSPA1A*, *HSPA1B*, *HSPA5* and *HSP90B1*).

**Statistical analysis.** For cell-based experiments, biological triplicates were performed in each single experiment in general, unless otherwise stated. For animal studies, no less than five replicates per group were performed. Animals were randomized into different groups after tumour cell inoculation. The investigators were not blinded to allocation during experiments and outcome assessment. Data are shown as mean values ± s.d. Statistical analysis was performed using GraphPad Prism 8 (GraphPad Software), following the manuals of GraphPad Prism 8.0 and an online resource (http://xena.ucsc.edu/). Two-tailed two-sided *t*-tests were used to compare treatment groups with control groups; survival function was estimated using the Kaplan–Meier methods and log-rank tests were used to calculate statistical differences.

**Reporting Summary.** Further information on research design is available in the Nature Research Reporting Summary linked to this article.

## Data availability

The RNA-seq data (GSE99299) and processed single-cell data (GSE123814) were obtained from Gene Expression Omnibus (GEO). The MS proteomics data (PXD006003) were obtained from PRIDE repository. The TCGA cancer datasets were obtained from UCSC Xena (http://xena.ucsc.edu/). The RNA-seq data and clinical information for immune checkpoint blockade clinical trials were provided by the respective corresponding authors. All raw data supporting the findings of this study are available from the corresponding author on request. Source data are provided with this paper.

## Acknowledgements

We thank members of the Zou laboratory for intellectual input. This work was supported in part by the research grants from the US NIH/NCI R01 grants (CA217648, CA123088, CA099985, CA193136, CA152470, to W.Z.; and CA216919, CA213566, CA120458; to M. Cohen), and the NIH through the University of Michigan Rogel Cancer Center Grant (CA46592).

## Author contributions

G.L. and W.Z. conceived the idea, designed the experiments and composed the paper. G.L. conducted experiments. I.K. assisted in FACS analysis. J.N., S.W., S.G. and L.V. assisted in animal experiments. X.L., S.L. and J.L. assisted in bioinformatics analysis. J.Z., W.D., H.L., T.W., C.S., J.J.M., M. Cieslik and M. Cohen contributed to the interpretation of the results. W.Z. supervised the project.

## Competing interests

W.Z. has served as a scientific advisor or consultant for NGM, Cstone, Oncopia and Hengenix. All of the other authors declare no competing interests.

## Additional information

**Extended data** is available for this paper at https://doi.org/10.1038/s41556-021-00672-3.

**Supplementary information** The online version contains supplementary material available at https://doi.org/10.1038/s41556-021-00672-3.

**Correspondence and requests for materials** should be addressed to W.Z.

**Peer review information** *Nature Cell Biology* thanks Weiyi Peng and the other, anonymous, reviewer(s) for their contribution to the peer review of this work. Peer reviewer reports are available.

**Reprints and permissions information** is available at www.nature.com/reprints.

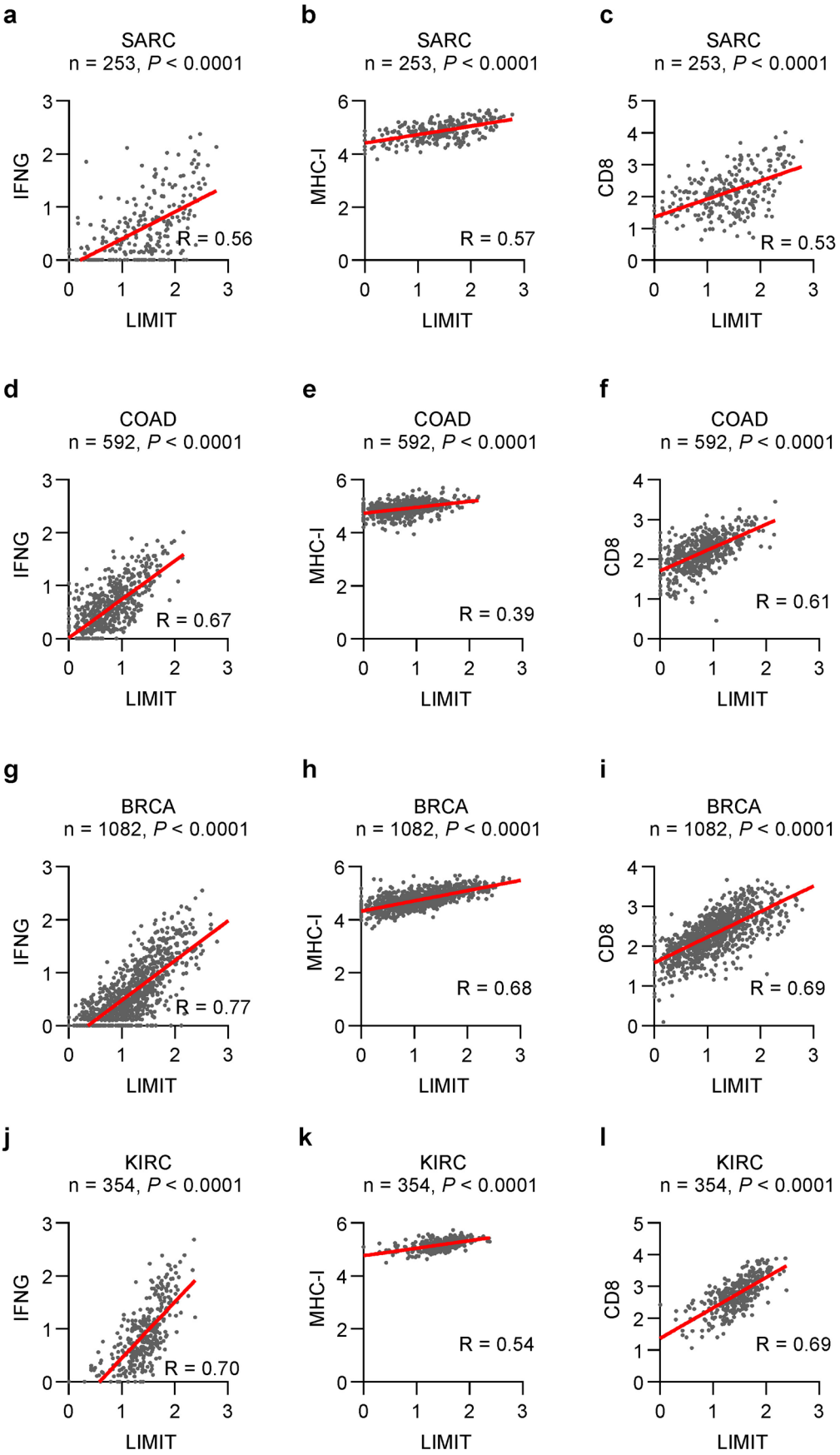


**Extended Data Fig. 1 | See next page for caption.**

**Extended Data Fig. 1 | LIMIT correlates to effector immune genes across multiple cancer types. a-l**, Correlation of LIMIT with IFNG, MHC-I, or CD8 in human patients with sarcoma (SARC) (**a-c**), colon cancer (COAD) (**d-f**), breast cancer (BRCA) (**g-i**), and kidney cancer (KIRC) (**j-l**). P value by 2 sided linear regression. Source data are provided.

**a**

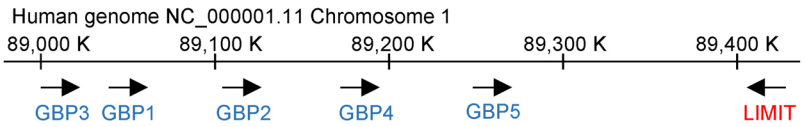


>Human-LIMIT (6 exons, 1967nt)

tctaaatccattacaaatatgcttaacctttaaatatttcatcactgaagaaatcccagccctacaacgttggaacagtaaaatattagtccaaggatccagtgagagacacagaagtgctagaagccactcctcat
gaactaaggagaaaaagaacagacaagggaacaccccagacatggtatcagagatccacatgacaggcccaatgtgcctcattgagaacactaatgggcgactgatggcgaatccagaagctctgaagat
cctttctgccattacgcagcctgtggtggtggtggcgactgtgggccgctagcgcacaggaaaatcctacctgattaacaagctggctcagaagaaaaagggcttctctctgggctccacagtgcagtctcacact
aaaggaatctggatgtggtgtatgccccatcccaagaagccaggccacatcctagttctgctggacaccgagggtctgggagatgtagagaagggtgacaaccagaatgactcctggatcttcgccctggccgt
cctcctgaacagcacttccatgtacaatagcataggaaccattaaccagcaggccatggaccaactgcagtatcctttgtgacccagaacagcaccaaggtcagagggcacctgtgttcataaaccagctgcct
gactgtgaatcctgatgaatcaagctcaaaaggagaaaacataaaatacataaagtacagaggagtgatcccatatatccactttagacttgacacttaggttaagaacaaaggaaaatggaaggtttgggaat
gtgttgaactaatatgggatgaggtccatgttcattttgtcacatttctttagttagctactcagctatgtgacagagctgacacatcgagtccaaccaaaatcttcacctgatgagaatgagaatgaggattcagctga
ctttgagagcttcttcccagactttgtgttgacactgagagatttctagcattacagaaagcgcttttggacaaaactgtgataaaataaactaaatggaggacttttttttattggaatagtttcatttgtttcatacatattga
tcaaatgcttactatgaatagactgaagatacagatataaatgaaatagatatggttcctgtcctaatgttgcttggggttaaaatggatgcaaacattcaattaacacaggtctatgtaatctagtacaagaactctca
aatgttggtatgcatacgtatcttctgaggatcttaccaaagacaaaagtctaattcaatagatcttggacagggtctaagagtctgtatttctgaaaaaaaaaaaaaaaaaaaaaaaaaaaaaagaattacaggg
aatagagactttctttactacaagaaacattagcatttgttctccataggcaggtctagagagcctggtgctgacctatgtcaatgccatcagcagtggggatctaccctgcatggagaacgcagtcctggccttggc
ccagatagagaactcagccgcagtgcaaaaggctattgcccactatgaaaagcagatgggccagaaggtgcagctgcccacagaaaccctccaggagctgctggacctgcacagggacagtgagagcaa
ggccactgaagttttcatcaggagttccttcaaagatgtggaccatctatttcaaaaggagttagcggtaatttttgtctcaaatttatatggtttagggtcatggaagacaaagtactacaaagaaagaaaacgagta
ttattttgatagaagtaattcttcctagctttcataatggtgacaacaacagatttgtaatcacatcaatcaagaggaccaactgtattattacagactcaaagttttaaaacatttttttcctgaataattttccctttacctaaa
tgcatacaactgataaccagagcttctaataaaattacctgcccactct

**b**

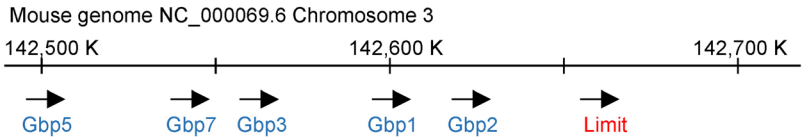


>Mouse-Limit (7 exons, 1634nt)

agaagacaaggagtgctggctccatcagagtctcggatagtggaggaccggccaccattgtgatttcacagagactcagagacaagtagaggaacaggaaacgttcattgtggaaggaagctccaggtcag
gtttttccatgggctccactgtgcagtctcaaaccaggggcatctggatgtggtgtgtgcctcatcccgagaaacctgaccacaccctagttctggatgacaccgagggcctaggagatgttgagaaagggtgaca
accagaacgactgctggatctttgccctggctatacttctaagcagcacctttgtctacaacagcatcggggccatcaaccagcaggccatggaccagctgcagtatctatgtgacagagctgactgacagaatc
agaacaagacgctcccctgaccatcaagctttggaggactcagatgaatatgtgagcttcttcccagactttgtatggaccccgagagacttctgtcttgagctgaaaacaaatggacaacccctctcagcagacg
aatacctagggaattccctgaagcttcttcaaggttctaggttgtagtcaaaaagaaaaagagttaaatctgtctcagctctgtatccgtaaattcttcccaactaagaaatgctttgtctttgagcgcccagcacccgg
gaagaagattggccagctggaatcactacaggataaagacctggactctgacttcgtgaaacaagtggcagagttctcttcctatgttttcaggtcttccaagattaaaaaaattccaggagacctcaaggtcaatg
gaccgcggactaaagaatttggtgacaacctatgtgaacaccatcagcaatgggtctctgccctgcatggagagtgctgtcctggctctgtcagaaacagagaactcagcagcagtgcgaaaggccattgccc
actatgaccagcagatgagccagagtctgaagctgcccacagagaccctccaggagctgctggacctgcacaggagcagtgagaaagaagccatcaagattttcatggaaaattccttcaaagatgttgacc
aagtgttcctaacaaaattagagattaaagacggaattagaaagaaggcaagcaaagggaattctgtaagaagaatcaagaggcatcctcagatcgctgttcagttctgcttcgggatatttttggtccactagaa
gaagacttgaagcagggtgtttttttacaaaccaacgggttgctgtcttttcagccagaagatacaggggttgaagagaaagtatgaggaacctgggaagggcgcaggtaaccaaggtaaccaaggttccgcat
gccctgggaagtttcttaccatcaggctgcagtgtccccaggcatcactggggaacgccagcttatgctgttcgtgtatcacatacctgaaggtcttcatactggatatttcctgctcacccatcagagacagtcactc
acttaacagtcagacagtcactcgcttaacaactgagctcaaactgaccaccttagccaccagtgggactgtcaccctctgtttcagctagactctttatgttgcaaagaactcaatggcaacccccttaaacaaaac
ttataattc

**c**

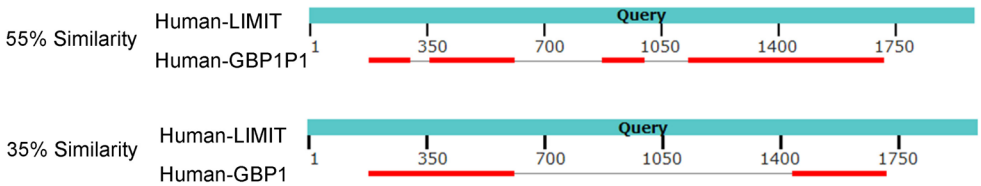


**Extended Data Fig. 2 | Genetic loci and sequences of human LIMIT and mouse Limit. a-b**, Genetic locus and genomic sequence of human LIMIT (**a**) or mouse Limit (**b**). **c**, Blast alignment of human LIMIT with GBP1P1 or GBP1.

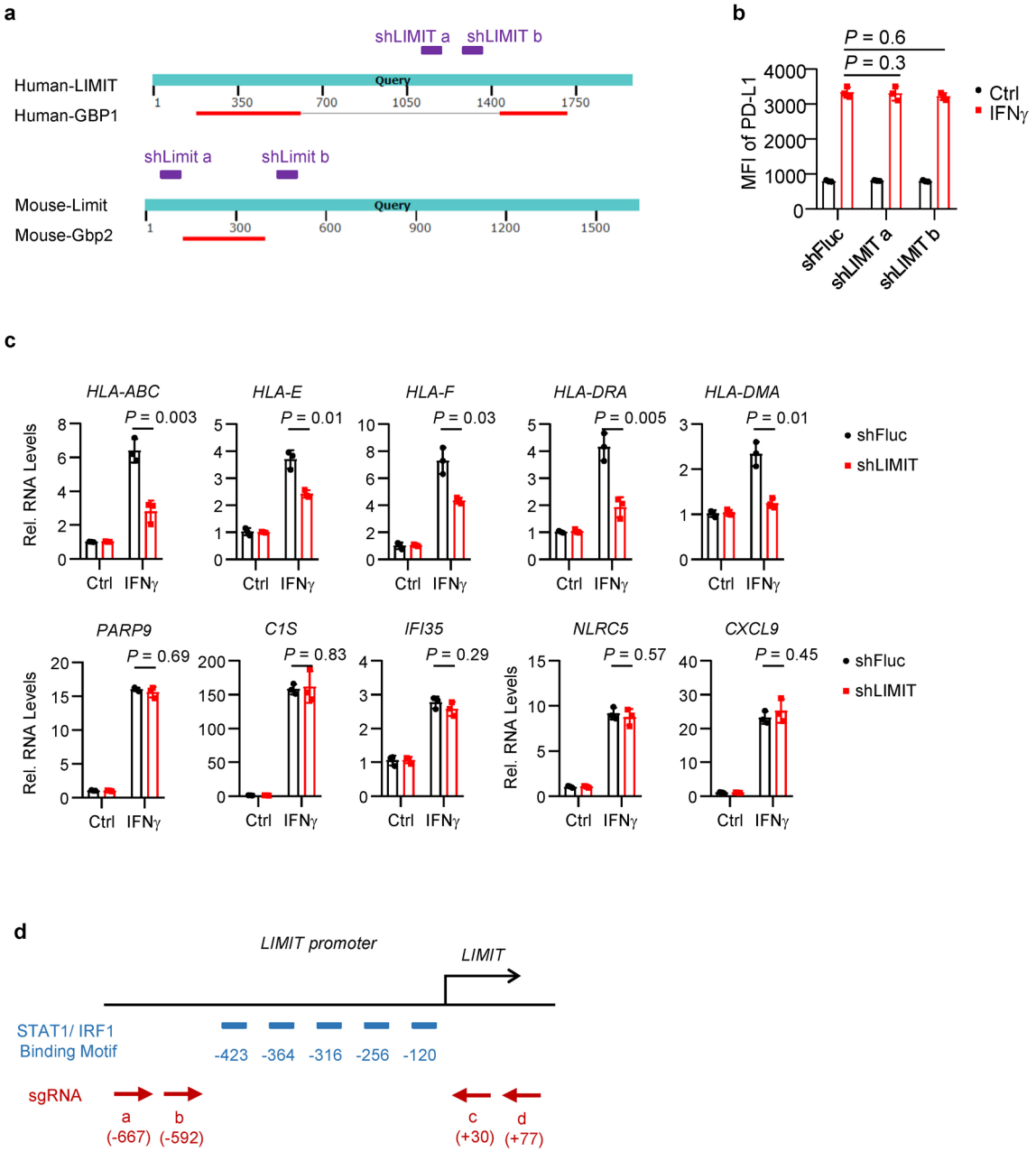


**Extended Data Fig. 3 | LIMIT augments MHC-I expression. a**, Schematic diagram showing the alignment among LIMIT, GBP, and shLIMIT. The shLIMIT target sequences are not present in GBP coding genes. **b**, A375 shFluc, shLIMIT a, and shLIMIT b cells were treated with IFNγ for 48 hours. Surface expression of PD-L1 was determined by flow cytometry (FACS). mean ± SD, n = 3 biological independent samples, P value by 2-sided t-test. **c**, A375 shFluc and shLIMIT cells were treated with IFNγ for 24 hours. RNA levels of indicated genes were determined. mean ± SD, n = 3 biological independent samples, P value by 2-sided t-test. **d**, Schematic diagram of the LIMIT promoter. The locations of 5 STAT1/IRF1-binding motifs and 4 sgRNAs capable of deleting the STAT1/IRF1 binding sites are indicated. Source data are provided.

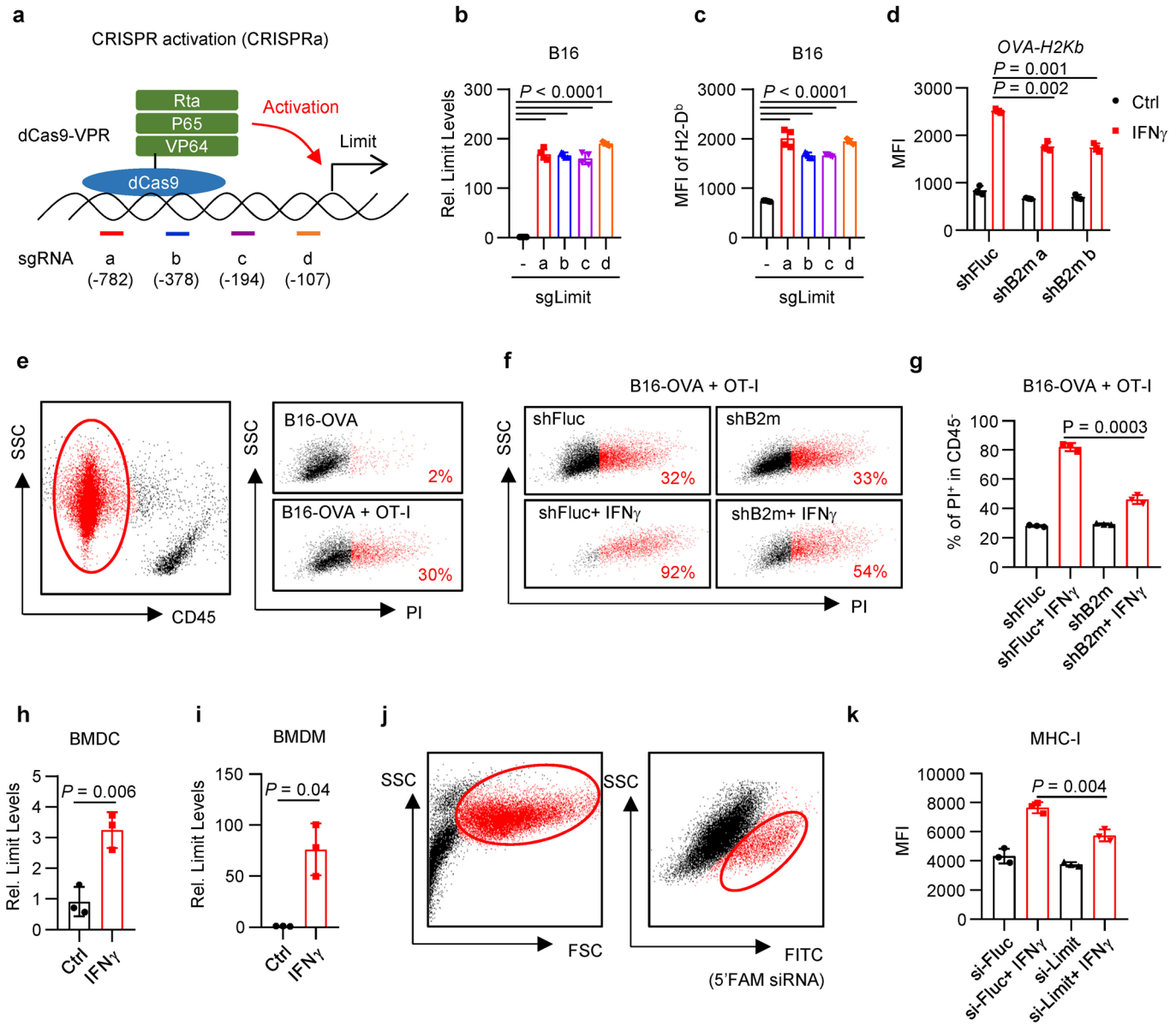


**Extended Data Fig. 4 | LIMIT augments MHC-I expression. a**, Schematic diagram of CRISPR activation targeting Limit. The transcriptional activator VPR was directed to the promoter of Limit by the interaction between guide RNAs and dCas9. **b-c**, B16 cells were transfected with dCas9-VPR alone or together with 4 sgRNAs. Subsequently, RNA levels of Limit (**b**) and surface expression of MHC-I (H2-D$^b$) (**c**) were detected 24 and 48 hours post transfection, respectively. mean ± SD, n = 4 biological independent samples, P value by 2-sided t-test. **d**, B16-OVA cells stably expressing shFluc, shB2m a, and shB2m b were treated with IFNγ for 48 hours. Surface expression of OVA-H2K$^b$ were determined by FACS. mean ± SD, n = 3 biological independent samples, P value by 2-sided t-test. **e**, B16-OVA cells were co-cultured with OT-I cell for 48 hours. Dot plots show the CD45$^-$ tumor cells. Tumor cell death was determined by PI staining. **f-g**, B16-OVA cells carrying shFluc or shB2m were co-cultured with OT-I cells at a 1:4 ratio. Cell killing was determined by PI$^+$ in CD45$^-$ tumor cells. Dot plots (**f**) and statistical results (**g**) are shown. mean ± SD, n = 3 biological independent samples, P value by 2-sided t-test. **h-i**, Bone marrow derived dendritic cells (BMDC) (**h**) or macrophages (BMDM) (**i**) were treated with IFNγ for 24 hours. RNA levels of Limit were determined by qRT-PCR. mean ± SD, n = 3 biological independent samples, P value by 2-sided t-test. **j**, BMDM were transfected with 5'FAM-labbled siRNA targeting Fluc or Limit. Dot plots show FSC vs. SSC and FITC vs. SSC gating. The FITC gating indicates the cells with positive siRNA transfection. 1 of 3 experiments is shown. **k**, BMDM were transfected with 5'FAM-labbled siRNA targeting Fluc or Limit, and treated with IFNγ for 48 hours. Surface expression of MHC-I (H2-D$^b$) were determined by FACS. mean ± SD, n = 3 biological independent samples, P value by 2-sided t-test. Source data are provided.

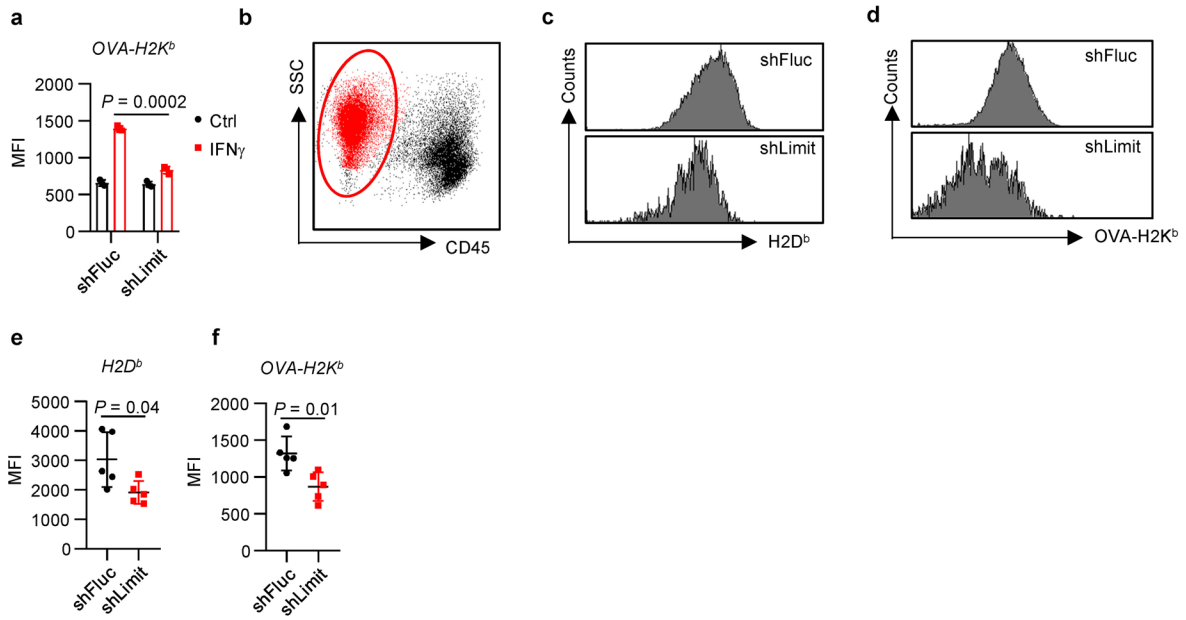


**Extended Data Fig. 5 | LIMIT augments antigen-loaded MHC-I expression in vivo. a**, YUMM1.7-OVA cells carrying shFluc or shLimit were treated with IFNγ for 48 hours. Surface expression of OVA-H2K$^b$ were determined by FACS. mean ± SD, n = 5 biological independent samples, P value by 2-sided t-test for end point tumor volume. **b**, Dot plot showing the CD45$^-$ gating of YUMM1.7-OVA tumor cells. **c-d**, Representative histogram showing the expression of H2D$^b$ (**c**) or OVA-H2K$^b$ (**d**) in YUMM1.7-OVA shFluc or shLimit tumor cells. **e-f**, Statistical results of H2Db expression (**e**) or OVA-H2K$^b$ expression (**f**) in YUMM1.7-OVA shFluc or shLimit tumor cells. mean ± SD, n = 5 biological independent samples, P value by 2-sided t-test. Source data are provided.

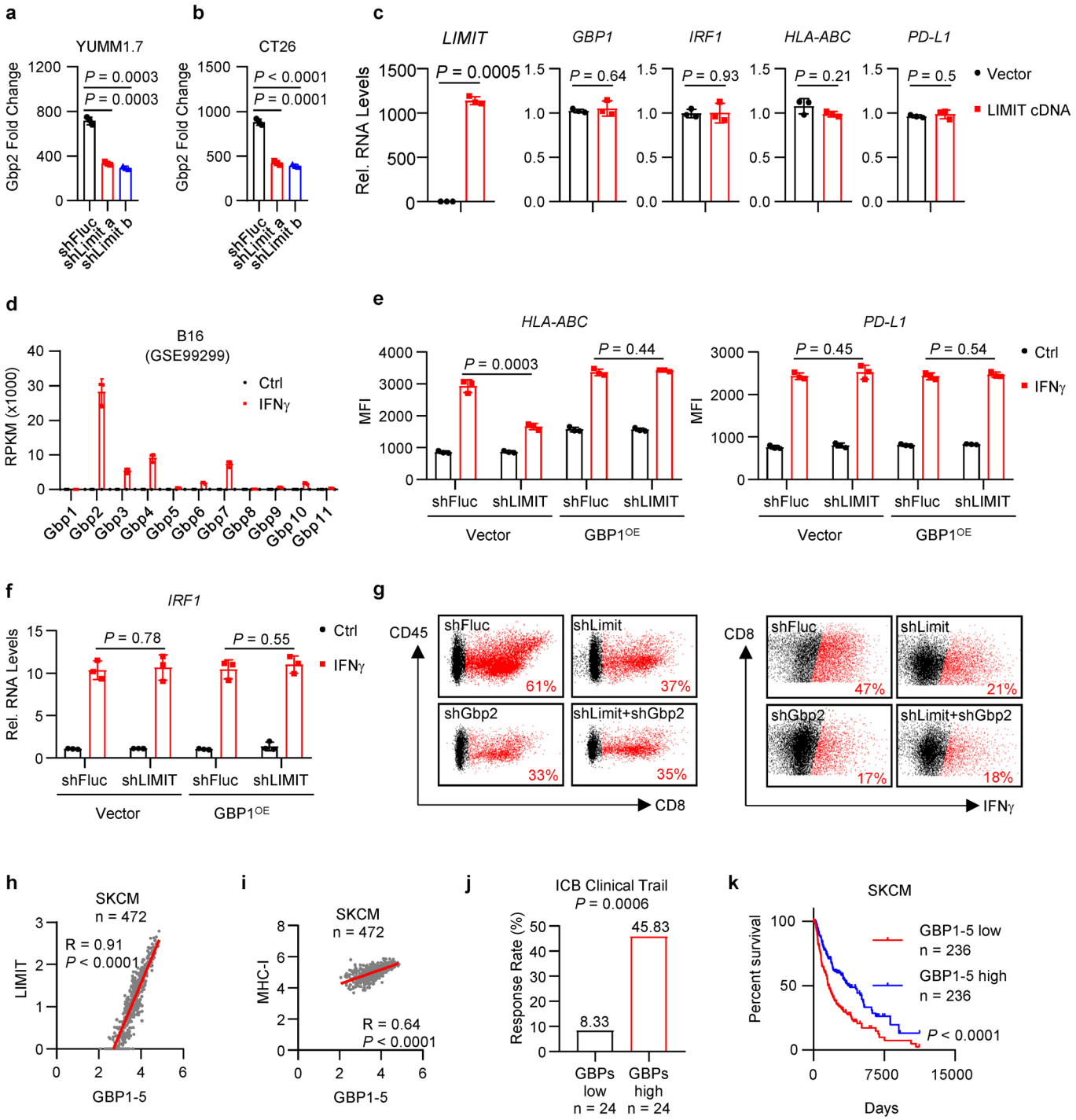


**Extended Data Fig. 6 | LIMIT cis-activates GBPs to boost MHC-I and tumor immunity. a-b**, Fold changes of Limit expression upon IFNγ treatment in YUMM1.7 cells (**a**) or CT26 cells (**b**) stably carrying shFluc, shLimit a, or shLimit b. mean ± SD, n = 3 biological independent samples, P value by 2-sided t-test. **c**, A375 cells were transfected with LIMIT cDNA for 24 hours. RNA levels of indicated genes were determined by qRT-PCR. mean ± SD, n = 3 biological independent samples, P value by 2-sided t-test. **d**, RPKM of Gbp family members upon IFNγ treatment in B16 cells (GSE99299). mean ± SD, n = 3 biological independent samples. **e**, A375 shFluc or shLIMIT cells were overexpressed with GBP1 ($GBP1^{OE}$), and treated with IFNγ for 48 hours. Surface expression of HLA-ABC or PD-L1 were determined by FACS. mean ± SD, n = 3 biological independent samples, P value by 2-sided t-test. **f**, A375 shFluc or shLIMIT cells were overexpressed with GBP1 ($GBP1^{OE}$), and treated with IFNγ for 24 hours. RNA levels of IRF1 were determined by qRT-PCR. mean ± SD, n = 3 biological independent samples, P value by 2-sided t-test. **g**, Dot plots of intral-tumoral $CD8^+$ T cell infiltration and activation in the YUMM1.7 tumors carrying shFluc, shLimit, shGbp2, or shLimit plus shGbp2. **h-i**, Correlations between GBP1-5 and LIMIT (**h**) or MHC-I (**i**) in human melanoma datasets. P value by 2 sided linear regression. **j**, Cancer patients having received ICB were divided into low and high GBP groups (bottom 15% vs top 15%). The response rates to ICB were calculated as the percentages of partial response (PR) plus complete response (CR). P value by Chi-square test. Patients were from 4 cohorts. **k**, Survival plot of patients with melanoma. Based on the expression levels of GBP1-5, patients were divided into high (top 50%) and low (bottom 50%) groups. P value by 2 sided log-rank test. Source data are provided.

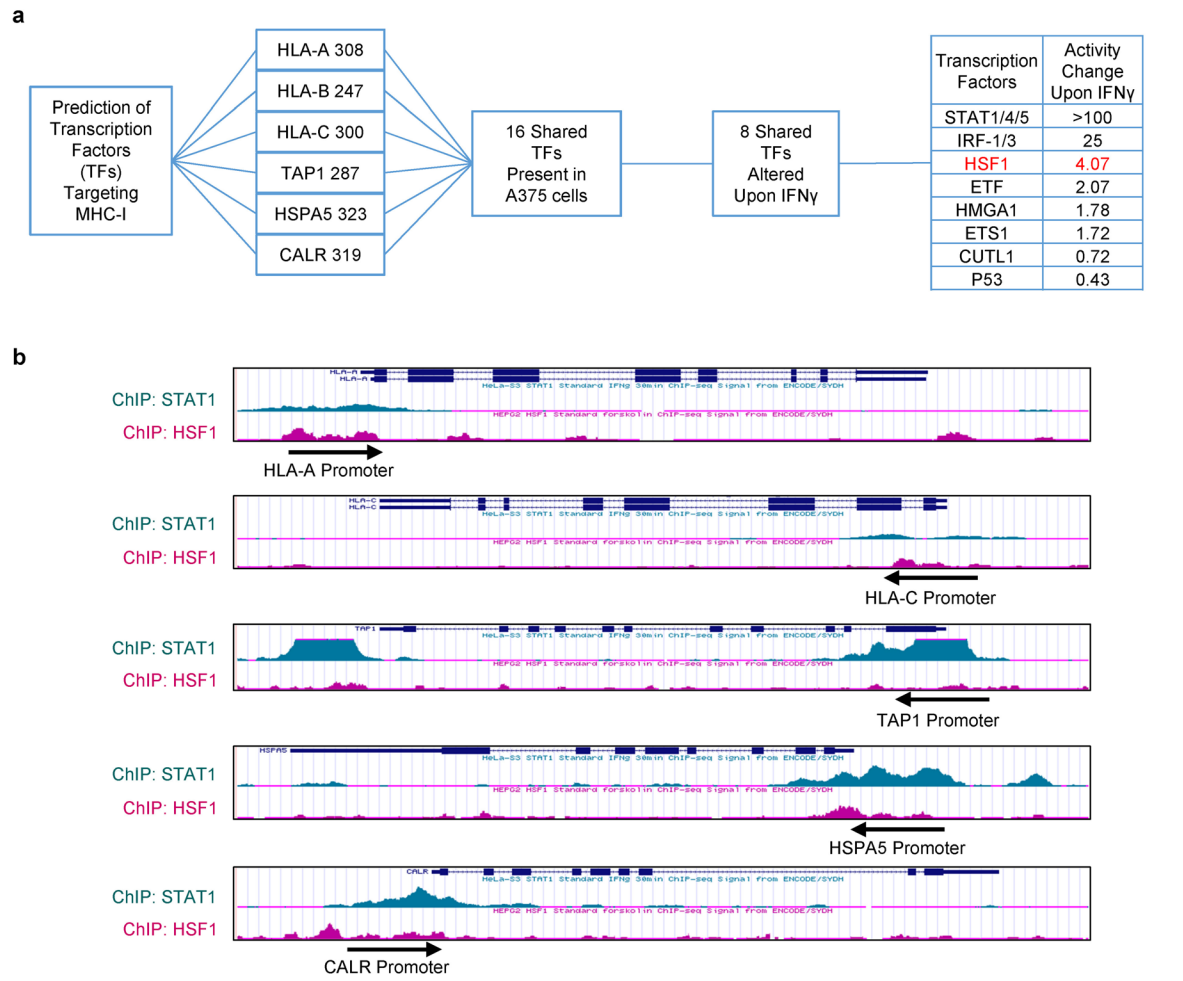


**Extended Data Fig. 7 | GBPs activate HSF1 to stimulate MHC-I expression. a**, Prediction of potential transcription factors targeting HLA-ABC, TAP1, HSPA5 and CALR. 8 shared transcription factors were altered by IFNγ in A375 cells (GSE99299). **b**, ChIP-seq results of STAT1 (Hela-S3 cells treated with IFNγ) or HSF1 (HepG2 cells in basal condition) derived from ENCODE at UCSC. The enrichment of STAT1 or HSF1 in the promoters of MHC-I related genes are shown. **c**, A375 cells were treated with multiple proteostasis stressors and KRIBB11. Surface expression of HLA-ABC was determined 48 hours after treatment. mean ± SD, n = 3 biological independent samples, P value by 2-sided t-test. **d**, Dot plots of IFNγ$^+$CD8$^+$ T cells or TNFα$^+$CD8$^+$ T cells in MC38 tumors carrying shFluc, shGbp2, shHsf1, and shGbp2 plus shHsf1. Source data are provided.

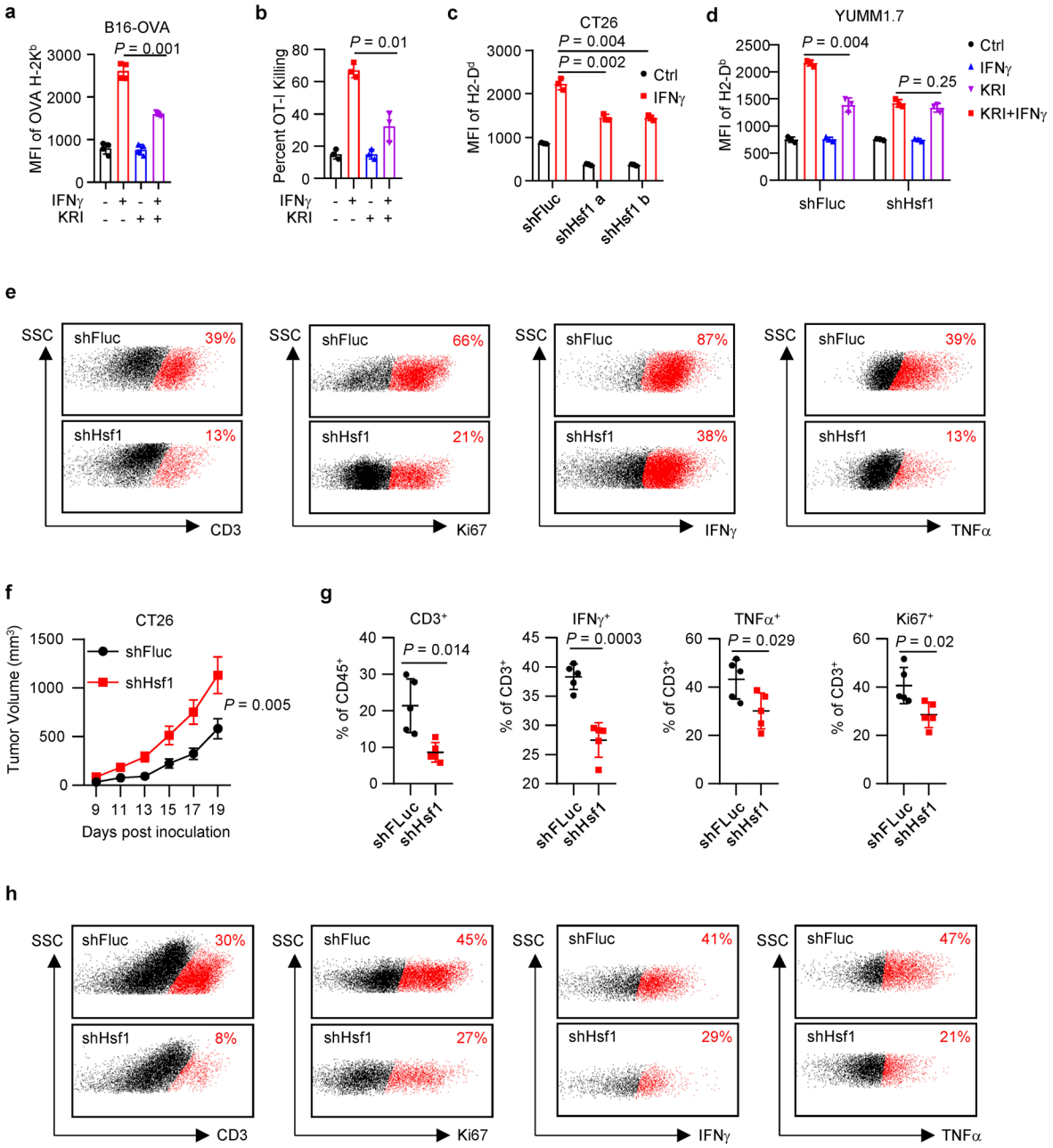


**Extended Data Fig. 8 | HSF1 drives MHC-I expression and tumor immunity. a**, B16-OVA cells were treated with IFNγ in the presence or absence of KRIBB11 for 48 hours. Cell surface expression of OVA-H2-K$^b$ was determined by FACS. mean ± SD, n = 4 biological independent samples, P value by 2-sided t-test. **b**, B16-OVA cells were pretreated with IFNγ in the presence or absence of KRIBB11 for 48 hours, then cultured with OT-1 T cells. Cell death was determined by 7-AAD staining in the CD45$^-$ tumor cells. mean ± SD, n = 3 biological independent samples, P value by 2-sided t-test. **c**, MHC-I (H2-D$^d$) surface staining of CT26 shFluc or shHsf1 cells treated with IFNγ for 48 hours. mean ± SD, n = 3 biological independent samples, P value by 2-sided t-test. **d**, YUMM1.7 shFluc or shHsf1 cells were treated with IFNγ in the presence or absence of KRIBB11 for 48 hours. Surface expression of MHC-I (H2-D$^b$) was determined by FACS. mean ± SD, n = 3 biological independent samples, P value by 2-sided t-test. **e**, Dot plots of CD3$^+$, Ki67$^+$, IFNγ$^+$, and TNFα$^+$ T cells in YUMM1.7 shFluc or shHsf1 tumors. **f**, Tumor growth curve of CT26 shFluc or shHsf1 tumors in BALB/c mice. mean ± SD, n = 6 animals, P value by 2-sided t-test for end point tumor volume. **g**, Percentages of CD3$^+$, IFNγ$^+$, TNFα$^+$, and Ki67$^+$ T cells in CT26 shFluc or shHsf1 tumors. mean ± SD, n = 5 biological independent samples, P value by 2-sided t-test. **h**, Dot plots of CD3$^+$, Ki67$^+$, IFNγ$^+$, and TNFα$^+$ T cells in CT26 shFluc or shHsf1 tumors. Source data are provided.

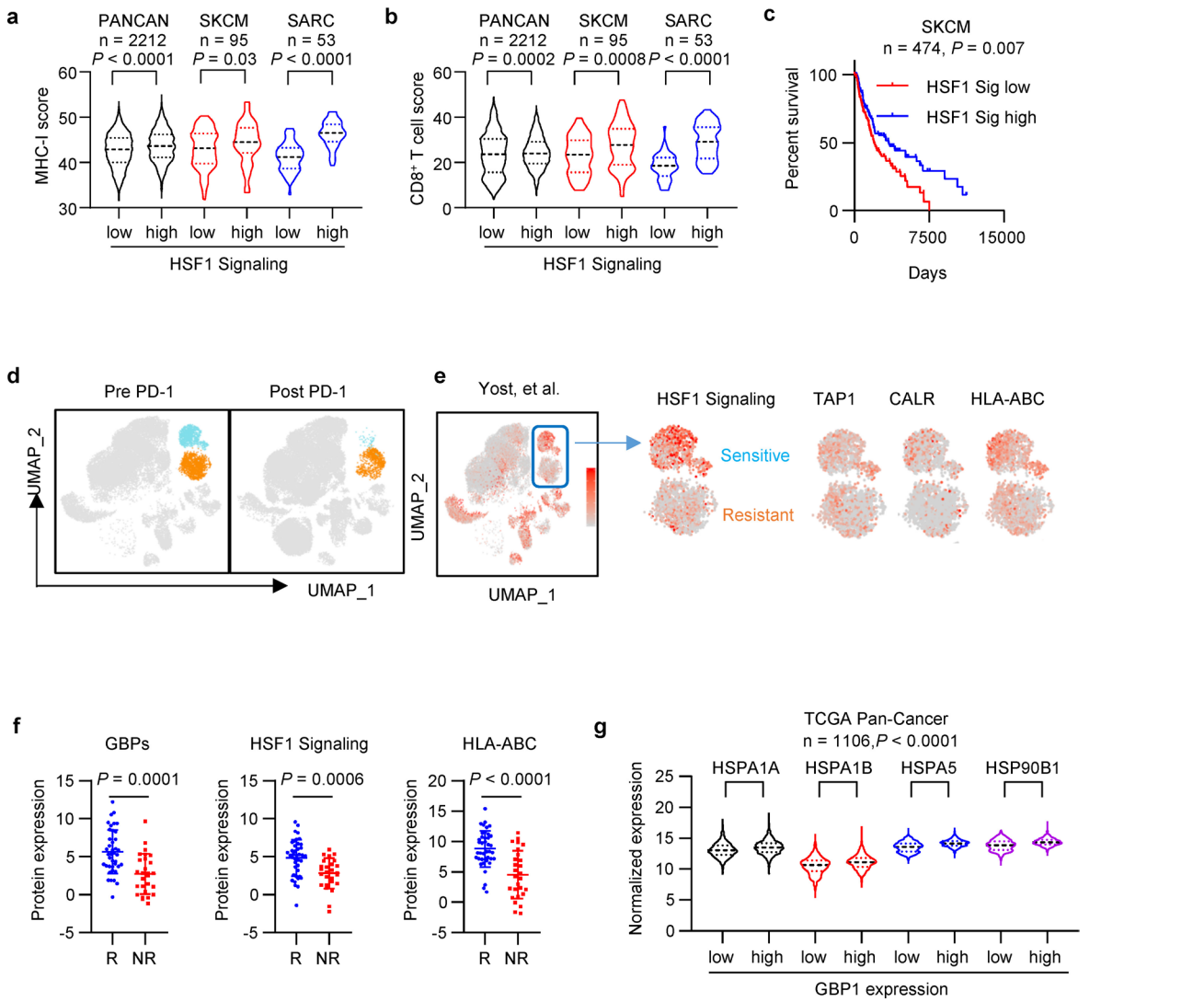


**Extended Data Fig. 9 | LIMIT-GBP-HSF1 axis drives MHC-I and tumor immunity and immunotherapy. a-b**, HSF1 signaling genes correlated with MHC-I expression (**a**) or CD8+ T cell infiltration (**b**) in Pan-Cancer (TCGA, PANCAN), melanoma (TCGA, SKCM) or sarcoma (TCGA, SARC). P value by 2-sided t-test. The minima, 25% percentile, median, 75% percentile, maxima for each blot are (**a**) (31.53, 40.0075, 42.87, 45.4925, 53.58), (32.02, 41.1175, 43.66, 46.205, 55), (31.82, 39.785, 43.16, 46.31, 50.39), (33.35, 42.215, 44.53, 47.55, 53.41), (32.9, 38.88, 41.19, 43.21, 47.55), (39.33, 44.75, 46.57, 48.4, 51.3); (**b**) (3.75, 15.6825, 23.6, 30.48, 49.23), (5.47, 19.5875, 24, 29.1525, 45.42), (7.711, 15.7925, 23.415, 29.7395, 39.722), (4.9254, 18.95, 27.857, 34.862, 47.79), (7.7582, 14.727, 18.553, 22.16, 36.084), (15.024, 22.149, 29.1, 35.582, 43.432). **c**, Survival plots of human melanoma patients (TCGA, SKCM). Based on the expression of HSF1 signaling genes, patients were divided into high (n = 150 patients) and low (n = 150 patients) groups. P value by 2-sided log-rank test. **d**, Single cell RNA-seq derived cell clusters pre- or post- anti-PD-1 therapy in human skin basal cell carcinoma. Two malignant clusters are denoted by color and show different sensitivities to PD-1 blockade. **e**, Expression of HSF1 signaling genes and MHC-I related genes in the single cell clusters prior to PD-1 blockade therapy. The therapy sensitive tumor cell cluster exhibited higher levels of HSF1 signaling genes and MHC-I related genes as compared to the therapy insensitive tumor cell cluster. **f**, Proteomics analysis in melanoma patients having received ICB. Protein expression of GBPs, HSF1 signaling genes, and HLA-ABC were compared in responders (R, n = 40 patients) and non-responders (NR, n = 27 patients). P value by 2-sided t-test. **g**, Based on the transcript levels of GBP1, human Pan-Cancers were divided into high (top 10%) and low (bottom 10%) groups. HSF1 target gene transcripts were plotted. mean ± SD, n = 1106 patients, P value by 2-sided t-test. The minima, 25% percentile, median, 75% percentile, maxima for each blot are (9.12, 12.29, 13.01, 13.8075, 18.2), (9.24, 12.73, 13.47, 14.19, 19.16), (5.32, 9.64, 10.625, 11.39, 15.74), (6.98, 10.365, 11.11, 11.78, 16.96), (10.86, 12.83, 13.59, 14.16, 16.68), (11.75, 13.77, 14.16, 14.5, 16.71), (10.57, 13.11, 13.84, 14.48, 16.33), (12.15, 13.96, 14.3, 14.71, 17.76). Source data are provided.

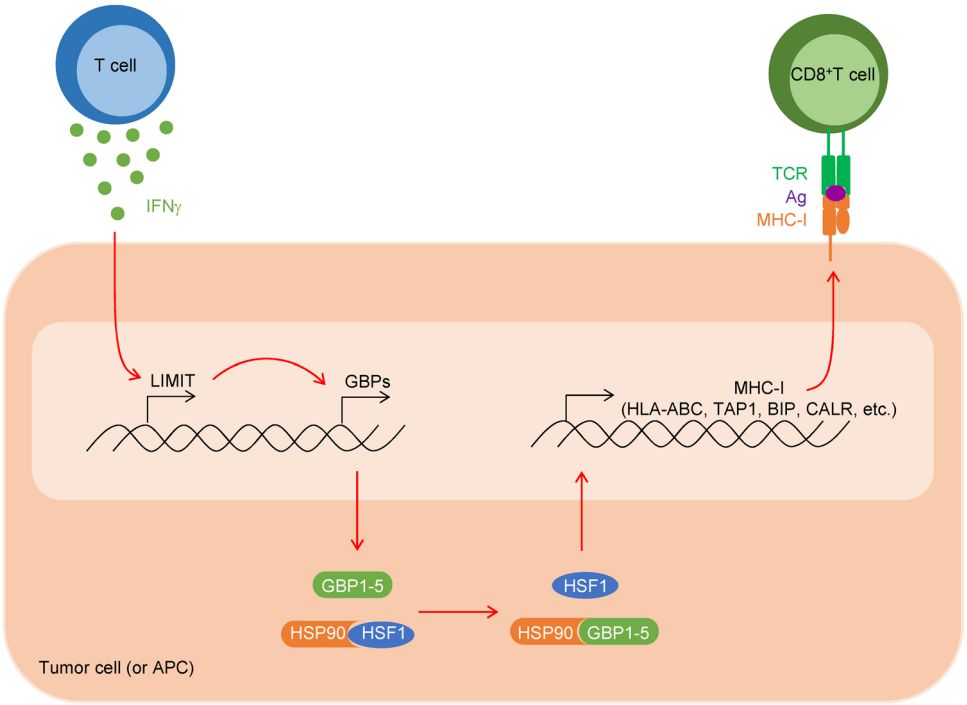


**Extended Data Fig. 10 | Scheme showing how LIMIT-GBP-HSF1 axis affects MHC-I and tumor immunity.** Cancer cells (or APCs) express LIMIT in response to IFNγ, thereby locally promoting the transcription of GBPs. GBPs interact with HSP90 and release HSP90-decoyed HSF1, resulting in HSF1 activation. Activated HSF1 stimulates the transcription of MHC-I and MHC-I related genes. MHC-I machinery mediates TAA-recognition and T cell activation, eliciting antitumor immune response.

nature research

Corresponding author(s): Weiping Zou

Last updated by author(s): Mar 24, 2021

# Reporting Summary

Nature Research wishes to improve the reproducibility of the work that we publish. This form provides structure for consistency and transparency in reporting. For further information on Nature Research policies, see our Editorial Policies and the Editorial Policy Checklist.

## Statistics

For all statistical analyses, confirm that the following items are present in the figure legend, table legend, main text, or Methods section.

| n/a | Confirmed | |
|---|---|---|
| ☐ | ☒ | The exact sample size (*n*) for each experimental group/condition, given as a discrete number and unit of measurement |
| ☐ | ☒ | A statement on whether measurements were taken from distinct samples or whether the same sample was measured repeatedly |
| ☐ | ☒ | The statistical test(s) used AND whether they are one- or two-sided<br>*Only common tests should be described solely by name; describe more complex techniques in the Methods section.* |
| ☐ | ☒ | A description of all covariates tested |
| ☐ | ☒ | A description of any assumptions or corrections, such as tests of normality and adjustment for multiple comparisons |
| ☐ | ☒ | A full description of the statistical parameters including central tendency (e.g. means) or other basic estimates (e.g. regression coefficient) AND variation (e.g. standard deviation) or associated estimates of uncertainty (e.g. confidence intervals) |
| ☐ | ☒ | For null hypothesis testing, the test statistic (e.g. *F*, *t*, *r*) with confidence intervals, effect sizes, degrees of freedom and *P* value noted<br>*Give P values as exact values whenever suitable.* |
| ☒ | ☐ | For Bayesian analysis, information on the choice of priors and Markov chain Monte Carlo settings |
| ☒ | ☐ | For hierarchical and complex designs, identification of the appropriate level for tests and full reporting of outcomes |
| ☒ | ☐ | Estimates of effect sizes (e.g. Cohen's *d*, Pearson's *r*), indicating how they were calculated |

*Our web collection on statistics for biologists contains articles on many of the points above.*

## Software and code

Policy information about availability of computer code

| | |
|---|---|
| Data collection | BD LSRII or LSRFortessa flow cytometer was used to run samples and data was acquired and analyzed by BD FACS Diva software (Ver.8.0.1). |
| Data analysis | Flow cytometry data were analyzed with BD FACS Diva software (Ver.8.0.1)<br>GraphPad Prism (Ver.8.0.0) were used for data analysis. |

For manuscripts utilizing custom algorithms or software that are central to the research but not yet described in published literature, software must be made available to editors and reviewers. We strongly encourage code deposition in a community repository (e.g. GitHub). See the Nature Research guidelines for submitting code & software for further information.

## Data

Policy information about availability of data

All manuscripts must include a data availability statement. This statement should provide the following information, where applicable:

- Accession codes, unique identifiers, or web links for publicly available datasets
- A list of figures that have associated raw data
- A description of any restrictions on data availability

The RNA-seq data (GSE99299) and processed single cell data (GSE123814) were obtained from Gene Expression Omnibus (GEO). The MS proteomics data (PXD006003) were obtained from PRIDE repository. The TCGA cancer datasets were obtained from UCSC Xena (http://xena.ucsc.edu/). The RNA-seq data and clinical information for ICB clinical trials were provided by the respective corresponding authors. All raw data supporting the findings of this study are available from the corresponding author on request. Source data are provided with this paper.

# Field-specific reporting

Please select the one below that is the best fit for your research. If you are not sure, read the appropriate sections before making your selection.

☒ Life sciences ☐ Behavioural & social sciences ☐ Ecological, evolutionary & environmental sciences

For a reference copy of the document with all sections, see nature.com/documents/nr-reporting-summary-flat.pdf

# Life sciences study design

All studies must disclose on these points even when the disclosure is negative.

| | |
|---|---|
| Sample size | No sample size calculation was done either for in vivo or in vitro studies. For in vivo studies, n =5-10 mice per group is sufficient to detect meaningful biological differences with good reproducibility. For in vitro studies, all experiments were replicated at least for 3 independent biological samples. We determined the sample size to be sufficient based on our experience and previously studies on tumor and cell models. |
| Data exclusions | No data were excluded from the manuscript. |
| Replication | As reported in the figure legends, the findings were reliably reproduced. |
| Randomization | For in vivo experiments, animals were randomized based on tumor burden before they were assigned into different treatment groups, to make sure the starting tumor burden in different treatment groups was similar before treatment. All groups were age and sex matched. For in vitro studies, cells were seeded, cultured and treated in triplicate wells and analyzed equally, therefore, no randomization were applied for in vitro experiments. |
| Blinding | Preclinical experiments were not performed in a blinded manner as the investigator needed to know the treatment groups in order to complete the study. All data were acquired and analyzed by software with objective standard, thus blinding was not relevant to the study. |

# Reporting for specific materials, systems and methods

We require information from authors about some types of materials, experimental systems and methods used in many studies. Here, indicate whether each material, system or method listed is relevant to your study. If you are not sure if a list item applies to your research, read the appropriate section before selecting a response.

## Materials & experimental systems

| n/a | Involved in the study |
|---|---|
| ☐ | ☒ Antibodies |
| ☐ | ☒ Eukaryotic cell lines |
| ☒ | ☐ Palaeontology and archaeology |
| ☐ | ☒ Animals and other organisms |
| ☒ | ☐ Human research participants |
| ☒ | ☐ Clinical data |
| ☒ | ☐ Dual use research of concern |

## Methods

| n/a | Involved in the study |
|---|---|
| ☒ | ☐ ChIP-seq |
| ☐ | ☒ Flow cytometry |
| ☒ | ☐ MRI-based neuroimaging |

## Antibodies

| | |
|---|---|
| Antibodies used | Antibodies used for flow cytometry (1:50): Anti-CD45 (30-F11, BD Biosciences), anti-CD90 (53-2.1, BD Biosciences), anti-CD3 (145-2C11, BD Biosciences), anti-CD4 (RM4-5, BD Biosciences), and anti-CD8 (53-6.7, BD Biosciences) anti-Ki67 (B56, BD Biosciences), anti-TNF (MP6-XT22, BD Biosciences), anti-IFNγ (XMG1.2, BD Biosciences), anti-HLA-ABC (G46-2.6, BD Biosciences), anti-H2-Db (KH95, BD Biosciences), anti-H2-Dd (34-2-12, BD Biosciences), anti-OVA-H2-Kb (eBio25-D1.16, eBioscience), and anti-PD-L1 (MIH1, BD Biosciences).<br>Antibodies for western blotting: anti-human GBP1-5 (Santa Cruz, 166960, 1: 500), anti-HSF1 (CST, 12972, 1: 1,000), anti-Phospho-HSF1 (Abcam, 76076, 1: 1000), anti-GBP1 (Proteintech, 15303, 1: 1,000), anti-Gbp2 (Proteintech, 11854, 1: 1,000), anti-HSP90 (CST, 4877, 1: 1,000), anti-HSPA5 (CST, 3177, 1: 1,000), anti-STAT1 (CST, 9172, 1: 1,000), anti-Phospho-STAT1 (CST, 9167, 1: 1000), anti-RAF1 (CST, 9422, 1: 1000), anti-BCL2 (CST, 2870, 1: 1000), anti-CDK4 (CST, 12790, 1: 1000), anti-GAPDH (Proteintech, 60004, 1: 5,000), anti-HLA-ABC (W6/32, Novus Biologicals, 64775, 1: 1,000).<br>Antibodies for ChIP (1:100): Normal Rabbit IgG (CST, 2729), anti-HSF1 (CST, 12972).<br>For in vivo experiments: anti-PD-L1 (InVivoMAb, 10F.9G2) and control antibody (InVivoMAb, LTF-2) |
| Validation | All antibodies were well-recognized clones widely used in the field and purchased from reputable vendors. Each antibody used has been validated for its utilized purchase by the manufacturer, and this information is available on the manufacturer website. These antibodies are further validated internally and routinely used in our lab. |

## Eukaryotic cell lines

Policy information about cell lines

| | |
|---|---|
| Cell line source(s) | Human melanoma cell line A375 (CRL-1619), mouse melanoma cell lines, B16-F0 (CRL-6322) and YUMM1.7 (CRL-3362), mouse colon cancer cell line CT26 (CRL-2638), and 293T (CRL-3216) were purchased from the American Type Culture Collection (ATCC). Mouse colon cancer cell line MC38 was used previously in the Zou laboratory (ref. 23, 48). B16-OVA cells were established as previously reported (ref. 42). A375 STAT1 KO, A375 GBP1-5 KO, and A375 LIMIT promoter deletion cell lines were generated in this study. |
| Authentication | Cell lines were not authenticated. |
| Mycoplasma contamination | All cell lines in our laboratory are routinely tested for mycoplasma contamination and cells used in this study are negative for mycoplasma. |
| Commonly misidentified lines (See ICLAC register) | No cell line used in the paper is listed in ICLAC database. |

## Animals and other organisms

Policy information about studies involving animals; ARRIVE guidelines recommended for reporting animal research

| | |
|---|---|
| Laboratory animals | Six- to eight-week-old female NSG (NOD.Cg-Prkdcscid Il2rgtm1Wjl/SzJ, Stock# 005557), C57BL/6 (C57BL/6J, Stock# 000664), BALB/c (BALB/cJ, Stock# 000651), and OT-1 (C57BL/6-Tg(TcraTcrb)1100Mjb/J, Stock# 003831) mice were obtained from the Jackson Laboratory. All mice were maintained under pathogen-free conditions. The animal room has a controlled temperature (18-23°C), humidity (40-60%), and a 12 light/12 dark cycle. |
| Wild animals | The study did not involve wild animals. |
| Field-collected samples | The study did not involve samples collected from field. |
| Ethics oversight | Animal studies were conducted under the approval of the Institutional Animal Care and Use Committee at the University of Michigan (PRO00008278). |

Note that full information on the approval of the study protocol must also be provided in the manuscript.

## Flow Cytometry

### Plots

Confirm that:

☒ The axis labels state the marker and fluorochrome used (e.g. CD4-FITC).

☒ The axis scales are clearly visible. Include numbers along axes only for bottom left plot of group (a 'group' is an analysis of identical markers).

☒ All plots are contour plots with outliers or pseudocolor plots.

☒ A numerical value for number of cells or percentage (with statistics) is provided.

### Methodology

| | |
|---|---|
| Sample preparation | Cells were trypsinized and washed 1 time with MACS buffer (PBS, 2%FBS, 1mM EDTA). Surface staining was performed by adding antibodies to the cell suspension in 50 µl MACS buffer. After incubating for 30 minutes, cells were washed 1 time with MACS buffer and analyzed on BD Fortessa flow cytometer.<br>To quantify intratumoral T cells and T cell effector cytokine expression, single-cell suspensions were prepared from fresh tumor tissues by physically passing through 100 µm cell strainers. Immune cells were enriched by density gradient centrifugation. For cytokine staining, intratumoral immune cells were incubated in RPMI culture medium containing PMA (5 ng/ml), ionomycin (500 ng/ml), brefeldin A (1: 1000), and Monessen (1:1000) at 37 °C for 4 hours. Anti-CD45 (30-F11), anti-CD90 (53-2.1), anti-CD3 (145-2C11), anti-CD4 (RM4-5), and anti-CD8 (53-6.7) antibodies were added for 20 minutes for surface staining. The cells were then washed and resuspended in 1 ml of freshly prepared Fix/Perm solution (BD Biosciences) at 4 °C overnight. After being washed with Perm/Wash buffer (BD Biosciences), the cells were stained with anti-Ki67 (B56), anti-TNF (MP6-XT22), and anti-IFNγ (XMG1.2) for 30 minutes, washed, and fixed in 4% formaldehyde (Sigma Aldrich). |
| Instrument | Data collection and analysis was performed on a LSR II equipped with four lasers or a BDFortessa equipped with four lasers (BD Biosciences). |
| Software | All data were analyzed with FACS DIVA software Ver.8.0.1 (BD Biosciences). |
| Cell population abundance | When cells were sorted or enriched, the purity was confirmed by flow cytometry and in each case the purity was above 90%. |
| Gating strategy | The cells were gated on FSC-A/SSC-A basis on the location known to contain lymphocytes. Doublets were excluded based on |

Gating strategy

FSC-A/FSC-H gating. CD45+ cells were gated for analysis of immune cells. Endogenous T cells were gated on CD45+CD3+CD90+ and analyzed for phenotype and cytokine production.

☒ Tick this box to confirm that a figure exemplifying the gating strategy is provided in the Supplementary Information.